APPLICATION OF BOUNDARY LAYER THEORY AND REYNOLDS NUMBER EFFECTS ON THE PERFORMANCE OF TURBOMACHINERY

Stephen K.W. Tou

A Dissertation

in

The Department

of

Mechanical Engineering

Presented in Partial Fulfillment of the Requirements
for the degree of Master of Engineering at
Concordia University
Montreal, Quebec, Canada

March, 1975

TABLE OF CONTENTS

LIST OF FIGURES

16 Compressor work factor as a function of percent design equivalent weight flow for various Reynolds Number.

17 Comparison of overall pressure ratio and flow range at various Reynolds Number for a 6" centrifugal compressor at design speed.

18 Massflow variation vs blade-chord Reynolds Number.

19 Overall performance of a 3.7" NASA six stage axial flow compressor.

20 Pressure ratio vs blade-chord Reynolds Number along the constant $\Delta T/T_1'$ locus.

Nomenclature

c	chord length
D	linear dimension of the machine
E	energy in mean flow
$\mathcal{E}$	energy in disturbance stream
f	friction coefficient
H	boundary-layer form factor
k	specific heat of gas
K	proportional constant
K_1	proportion constant
J	turbulence intensity
l^*	characteristic length
$\dot{m}$	mass flow
N	fluid properties
P	total pressure
ΔP	mass averaged loss in total pressure
R_c	Reynolds number based on chord length
R_δ	Reynolds number based on boundary layer thickness
R_x	flat plate Reynolds number
s	coordinate along direction of blade surface
t	time
T	total temperature
ΔT	temperature rise
V	air velocity
v	s-component of velocity in boundary layer
u	n-component of velocity in boundary layer
x	abscissa in cascade plane
y	ordinate in cascade plane
β	air angle, angle between air velocity and x-axis
λ	ratio of the length of the separated region to the boundary layer thickness
θ	boundary-layer momentum thickness
δ^*	boundary-layer displacement thickness
δ	boundary-layer thickness
μ	viscosity
ν	kinematic viscosity
σ	solidity, ratio of chord to spacing
η	efficiency
ρ	density
τ_w	shear stress at wall
$\bar{\omega}$	total pressure loss coefficient

Subscripts

AERO	aerodynamic
c	overall
OVERALL	
n	n-direction
o	outer edge of boundary-layer
p	polytropic
ref	reference
s	s-direction
shf	shaft
te	trailing edge
tr	transition
1	upstream at infinity
2	downstream at infinity

ABSTRACT

STEPHEN K.W. TOU

APPLICATION OF BOUNDARY LAYER THEORY AND REYNOLDS NUMBER EFFECTS ON THE PERFORMANCE OF TURBOMACHINERY

This report presents an attempt to assess results obtained from many published experimental works and to produce, in conjunction with theoretical analysis, more accurate means of estimating and predicting the onset and magnitude of high losses at low Reynolds number. It describes an investigation into the effects of Reynolds number on the flow through a two-dimensional turbomachine. The main work consists of approximate mathematical analysis of representative flows in a typical compressor geometry. The generally accepted approach for the development of the theoretical work has been followed in that the potential flow pattern has been used as a basis for further calculation of Reynolds number and boundary layer momentum thickness.

The general characteristics of laminar boundary layer development on the blade sections is first reviewed, and is followed by discussion on transition due to boundary layer instability. The performance of the machine at low Reynolds number is then explained in terms of the behaviour of the boundary layer attached to the blades. Transition from laminar to turbulent flow in the boundary layer is shown to be of vital importance

in determining the flow pattern especially at low Reynolds number where laminar breakaway is likely to occur. An attempt is made to construct a quantitative picture on the performance of a turbomachine in relation to the Reynolds number variation, surface pressure gradient and free stream turbulence.

A semi-empirical method of predicting critical Reynolds number at transition is presented. The correlation between the performance of a turbomachine and Reynolds number variation is established; it compares well with other published results.

It is shown that the Reynolds number effects are most pronounced when the flow enters the laminar regime where high losses are expected due to viscous dissipation of energy. It follows a .5 power law in the laminar region and a .1 power law in the turbulent region. If separation of the laminar layer takes place before the point of transition at low Reynolds number, the separated boundary layer might be so stable that reattachment of flow in a turbulent form is impossible and the performance could deteriorate rapidly. It is also shown that design criteria and methods can be modified to ensure improved performance at a specific Reynolds number or over a large range of Reynolds number.

ACKNOWLEDGEMENTS

The author wishes to express his gratitude to Professor duPlessis and Professor Lin for their supervision on the subject investigation and to his colleague Dr. Ma whose valuable suggestions were essential for the completion of this study.

1.0 INTRODUCTION

As the range of uses for gas turbine engines continues to expand, the need to know what effects variation in size and changes in the inlet conditions can have on performance becomes increasingly important. Small compressors, for example, are now being used in outerspace; conventional turbojets are also designed for flight at high altitudes where the Reynolds number is extremely small. According to the principal of similarity, all dimensionless parameters should be theoretically unvaried under tested conditions in order to have the expected performance. The performance of a turbomachine can be defined in terms of the achieved pressure ratio together with the associated values of total temperature rise and polytropic efficiency (Appendix I). It can be shown by dimensional analysis that these parameters are functions of nondimensional groups representing the pressure ratio (P_2/P_1), the rotor Mach number ($U/\sqrt{T}$), the flow coefficient ($\dot{m}\sqrt{T}/P$) and the Reynolds number (Rc) of this flow (Appendix I). In general, the first three parameters representing as they do the blade Mach number level, the flow Mach number level and the pressure ratio which are considered to be the predominant parameters controlling the performance, whereas the Reynolds number similarity is usually neglected. Under certain conditions, significant changes in performance can result from changes in the flow Reynolds numbers and it is these effects which are studied in this paper.

The performance of a wide variety of compressors, when tested over a range of Reynolds numbers, has been analysed in the past, in an attempt to produce a satisfactory correlation of the results. Two basic approaches to the problem of producing such a correlation have been followed (Reference 3,5 and 6). One is related to a knowledge of the detailed changes that take place within each stage in a compressor and could incorporate data derived from both cascade tests and interblade row measurements in an actual machine. The other is to assume that the rotating machine consists of a control volume, whose internal behavior and interactions can be neglected, but behaves in a consistent and repeatable manner dependent on the geometric parameters which define the control volume itself. In this analysis, the first approach is adopted to represent a qualitative discussion of boundary-layer behavior and at the same time to treat the quantitative aspects of boundary layer theory as applied to cascade blades. The second approach is also adopted in an attempt to correlate the experimental data empirically. The method of correlations in this report appear to be satisfactory for predicting of compressor performance and avoids considering the detailed flow changes that occur within the machine as the Reynolds number is varied.

2.0 OBSERVED EFFECTS OF REYNOLDS NUMBER VARIATION

Figure 1 shows the general characteristics of a compressor map in which the Reynolds number effect is shown.

The performance of a compressor is represented in terms of a series of constant speed "CHARACTERISTIC" each of which describes the stable ranges of operation of the machine at a given blade Mach number $(U/\sqrt{T})$. The upper boundary of each characteristic is determined by the complete breakdown of stable flow conditions and is known as the surge point, whereas the lower limit is controlled by the choking condition. A variation in the level of Reynolds number appears to produce a bodily shift in both the flow-pressure ratio and the efficiency (Appendix III) pessure characteristics as indicated in Fig. 1, with very little change in their shape. It is therefore necessary to define equivalent points on the characteristics for each level of Reynolds number so that any change in performance can be observed.

In order to remove any effects which might result from changes in operation of one stage relative to the next, it was decided to choose operating points at which the mean velocity triangles for the machine remain unchanged. This can be achieved approximately by considering operation of the machine at point of constant input power, that is, at a constant value of $C_p\ (\Delta T/T_1)$ (Appendix II). The changes in flow and efficiency parameters

have therefore been defined in relation to this criterion and are depicted in Figure 1. Since these changes are known as functions of Reynolds number, (Appendix I) it is possible to build up a new characteristic at any required level of Reynolds number from a measured characteristics. The changes in surge pressure ratio, however, need not correspond to a constant C_p $(\Delta T/T_1)$ since surge is essentially a phenomena associated with blade stalling. For this reason, the observed changes in the surge pressure ratio have been correlated regardless of the initial value of $C_p \Delta T/T_1$ to indicate the onset of instability.

Some published data obtained by Propulsion Research corporation (Ref. 3) are qualitatively quoted to further anticipated trends. Figure 2 indicates the variation of maximum efficiency, and peak pressure coefficient with Reynolds number. The distinct break in the data at the critical Reynolds number is noted. The slight shift in the critical Reynolds number is due to the fact that the above performance parameters do not occur at the same flow coefficient (Appendix I). Increasing the angle of incidence of the flow (decreasing flow coefficient) causes the critical Reynolds number to decrease slightly since the separation bubble moves to the leading edge. This observation can be further illustrated when the blades are operating towards stall. In this case, the critical Reynolds number tends to approach a minimum, resulting in a stable separated flow.

A review on the experimental results shows that the loss coefficient ($\bar{\omega}$) (Reference 5 and 8) increases very rapidly with decreasing Reynolds number in a way similar to the drag coefficient of a circular cylinder (Appendix IV). This is because in both cases the Reynolds number effect is due to the presence of boundary layer. When the flow eventually enters the laminar regime, the losses in the cascade will be mainly due to viscous forces provided that the pressure distribution outside the laminar boundary layer is of a kind which nearly prevents separation to take place. Based on these observations, the loss coefficient of a cascade should, in principal, bear the same basic characteristics of the skin-friction coefficient of a flat plate or a single airfoil. The following relation between the loss coefficient and the Reynolds number is therefore anticipated: (Reference 22 & Appendix VI)

$$\bar{\omega} \propto R_x^{-.5} \qquad \text{for laminar flow -----(1)}$$

and $\bar{\omega} \propto R_x^{-.2}$ for turbulent flow --(2)

where $= P/\frac{1}{2}\rho v_{ref}^2$

In the development of boundary layer on cascade blade sections, the primary consideration is whether the transition occurs before or after the point of laminar separation. The origin of turbulence and the accompanying transition from laminar to turbulent flow appeared to be of fundamental importance. To further this trend, the effect of transition location on the drag characteristics of submerged bodies is now graphically illustrated by the well-known flow around a sphere at a fixed turbulence level as represented in figure 3. At low Reynolds numbers, when no transition occurs, the laminar boundary layer separates and high profile drag results. When transition occurs before the point of laminar separation at relatively high Reynolds number, the resulting turbulent layer can tolerate a greater adverse pressure gradient; separation of the turbulent layer is delayed, and a lower profile drag is observed. The Reynolds number at which the rather sudden change of drag characteristic occurs, called the maximum critical Reynolds number of the sphere, corresponds to the point where the transition and separation coincide. (Appendix [illegible])

3.0 APPLICATION OF BOUNDARY LAYER THEORY IN TURBOMACHINERY

3.1 General Description of The Boundary Layer

Although, in many practical problems, the blade surface boundary layer constitutes a small portion of the flow field, it plays a decisive part in the determination of the actual flow characteristics. The effect of blade boundary layer development on cascade losses is recognized since the resulting wake formation (or flow separation) contains a defect in total pressure. If the boundary layer is very thin, the pressure distribution obtained from potential flow calculation could be a good approximation to the real flow. However, as the boundary layer thickens the actual distribution will depart from the potential flow calculation. Under certain conditions, the boundary layer may actually separate from the surface of the blade somewhere in advance of the trailing edge. When this happens, the entire flow pattern about the cascade is altered by the displacement of fluid accompanying such separation and the ideal fluid flow solution about the original profile is impossible.

In a conventional compressor design, laminar, transition and turbulent flow are all present. In the laminar regime, the dissipation of energy is confined within the boundary layer adjacent to the wall, while in the turbulent regime it takes place in a region of intense turbulent mixing and is not directly related to the friction at the wall. The behavior and loss characteristics in the laminar and turbulent flow regimes are markedly different due to the fact that viscous (skin friction) drag is predominating in the laminar flow, while the pressure drag is predominating in a turbulent and/or separated flow. Therefore the location and nature of the transition between the regions are significant in determining the magnitude of the resulting wake. One of the most important correlation in relating the boundary layer momentum thickness to the pressure loss coefficient has been established as below: (Ref. 5)

$$\bar{\omega} = 2\left(\frac{\theta}{c}\right)_{te} \frac{a}{\cos\beta_{2s}} \left[1 + \frac{1}{2}\left(\frac{\theta}{c}\right)_{te} \frac{a H_{te}}{\cos\beta_{te}}\right] \qquad (3)$$

Thus, the boundary layer momentum thickness at the blade trailing edge is considered herein as the basic parameter reflecting qualitatively the total pressure loss (or the total drag = viscous drag + pressure drag, see Appendix V & VI) for an isolated airfoil. The prediction of the loss characteristics of a given compressor geometry thus involves

an analysis of the composite effects of different boundary layer regimes. The principal factors affecting the boundary layer are the local surface pressure distribution (pressure gradient), the blade-chord Reynolds number and the free-stream turbulent level. (Ref.5) Other factors such as secondary flow and three dimensional effects are believed to be of secondary importance and hence neglected in the analysis that follows.

3.2 Laminar Boundary-Layer

The boundary layer equation was first developed by Von-Karman in the following form: (Ref. 5)

$$\frac{\tau_w}{\rho V_e^2} = \frac{d\theta}{ds} + \frac{\theta}{V_e}(2+H)\frac{dV_e}{ds} \qquad \text{——(4)}$$

It follows that the solution of viscous flow in a turbo-machinery requires the potential flow about the blade rows to be determined first (figure 4). In Ref. 10, Thwaites has developed equations (5 & 6) for predicting the growth and separation of the laminar boundary layer. They are:

$$\theta^2 = \frac{45\nu}{V_e^6}\int_0^s V_e^5\, ds \qquad \text{——(5a)}$$

and

$$m = \frac{\theta^2}{\nu}\frac{dV_e}{ds} \qquad \text{——(6)}$$

Where m = velocity distribution form factor

This method, developed from equation (4), results in a non-dimensional form parameter for the velocity distribution across the laminar layer, which is a function of velocity distribution in the main stream: Separation is expected to occur when this parameter reaches a given value (m = .082 Reference 13). According to this method, the position of the laminar separation point is primarily characterized by the boundary layer thickness and the local gradient of free stream velocity over the blade surface up to that point.

Hence, the value of 'm' at each point along the blade surface for a pressure distribution computed from the potential flow theory is unique and independent of the absolute magnitude of the velocity. This approximation is good only when the experimental velocity distribution remains close to the potential flow distribution regardless of Reynolds number variation. By rewriting equation (5a) in a non-dimensional form

$$\left(\frac{\theta}{c}\right)^2 = \frac{.45\nu \int_0^{\delta} V_1^6 \, d(\delta/c)}{c\, V_1^6} \quad ; \text{ with } Re_c = \frac{cV_1}{\nu}$$

$$\text{or} \quad \left(\frac{\theta}{c}\right)^2 = \frac{.45\nu \int_0^{\delta} (V_1/V_1)^6 \, d(\delta/c)}{c\, V_1 \, (V_1/V_1)^6} \qquad (5a)$$

$$\text{Let} \quad I = \left(\frac{\theta}{c}\right)^2 R_c = .45 \frac{\int_0^{\delta} (V_1/V_1)^6 \, d(\delta/c)}{(V_1/V_1)^6} \qquad (5b)$$

$$\text{We have} \quad \frac{\theta}{c} \propto \frac{I}{\sqrt{R_c}} \qquad (5c)$$

Rewrite equation (6) and substitute equation (5b) to obtain

$$m = -\left(\frac{\theta}{c}\right)^2 \frac{d(V_o/V_1)}{d(s/c)} \frac{V_o c}{\nu}$$

$$= -I \frac{d(V_o/V_1)}{d(s/c)} \qquad \text{——(5d)}$$

Equation (5d) indicates that laminar separation point is a function of local velocity gradient, momentum thickness and blade-chord Reynolds number. (Appendix V) Furthermore, separation will not occur until $d\ (V/V_o)$ becomes negative, ie, $\overline{d(s/c)}$

flow is being decelerated.

The values of 'm' along the suction surface (Appendix V) of the blade can be calculated as per equation (5d) and is presented in figure 5 as a function of surface distance. For separation to take place, we set m = .082 in equation (5d) to obtain

$$I = -.082 \Big/ \left[\frac{d(V_o/V_1)}{d(s/c)}\right] \qquad \text{——(5e)}$$

The value of 'I' is to be determined from the velocity gradient. (ie, the slope of V_o/V_1) vs (S/C) as shown in Fig. 4)

The pronounced effect of the surface velocity gradient on the calculated location of the point of laminar separation is illustrated in figure 5 for a typical Joukowski profile. The point of separation moves close to the point of peak velocity as a result of increased pressure gradient. It

is also observed in the above figure that the point of instability moves towards the trailing edge and approaches the point of laminar separation as the Reynolds number is decreased.

If transition to turbulent flow takes place before the laminar separation point is reached, separation of the laminar layer will not occur and the local pressure rise will be maintained (Appendix IV). If the transition moves back towards the trailing edge, as would result from a reduction of Reynolds number, separation will begin but will be arrested soon after the transition point when the boundary layer returns to the surface in the turbulent form. However, further movement of the transition point in a rearward direction allows separation to develop before the subsequent recovery in the turbulent layer and finally, a stage is reached at which breakaway is complete before transition resulting in no further rise of static pressure. The Reynolds number at this stage corresponds to the minimum critical Reynolds number resulting in a stable separated flow.

3.3 Transition Flow

For conventional airfoil shapes, the initial laminar boundary, if it remains laminar, will separate at some point downstream where the pressure is minimum. Therefore, transition to turbulent flow may or may not occur at a

point prior to the laminar separation point depending on the critical Reynolds number and the level of disturbance. The relative positions of laminar separation and transition are of great importance in deciding the performance of the blades. Although the exact mechanism causing the transition is not well known, the first and by far the most successful theoretical work on this subject has explained many fascinating phenomena associated with transition and has led to believe that proper disturbing frequencies within the boundary are a prerequisite for transition to take place. (Reference 5 & 10)

Basically, this theory was concerned with instability of the laminar boundary layer with respect to infinitesimal oscillation within the layer. In a stable laminar boundary layer the disturbances are damped, while in an unstable boundary layer the distrubances are amplified. The point of division called the neutral or instability point, depends on the origin of the disturbance. The existence of instability in a laminar boundary layer indicates that transition is possible but not necessarily after the neutral point. The actual transition to a fully developed turbulent motion will occur some distance downstream (Reference 5). ceording to this theory, an instability of the laminar boundary layer results from (1) viscous effects (2) boundary

layer thickening. The theory further indicates that the instability point is a function of the boundary-layer Reynolds number R_δ. Below some value of Reynolds number, infinitesimal oscillations are damped. This particular value is defined as the critical Reynolds number. On the other hand oscillations are amplified when the Reynolds number exceeds this critical Reynolds number.

The mathematical approach to the problem of transition has so far been limited to a study of the amplification of small disturbances in the laminar layer. In spite of the fact that the work on boundary layer theory and development by Dr. Schlichiting has had notable success in its agreement with experimental data (Reference 10), this approach has not yet reached the stage at which prediction of actual transition points in flows where pressure gradients are present may be undertaken. However, the instability theory has demonstrated that the change to turbulent flow appears to be gradual rather than a sudden occurrence. This suggests that transition is not merely a function of velocities distribution and boundary thickness at a particular point but also, in part, determined by the development of the boundary layer over a considerable part of the blade surface.

Coleman Dup. Donaldson (Ref. 1) has successfully computed the onset of transition from a set of modelling equations as shown in figure 7. The stable, neutral and unstable

regions are clearly defined and are compared to the classical linear stability theory.

3.4 Effect of Reynolds Number and Pressure Gradient on Transition

Following the preceding analysis, the instability value of the boundary layer Reynolds number will depend largely on the form of the velocity profile of the basic boundary-layer flow. This profile is determined primarily by the longitudinal pressure gradient. The greater the positive pressure gradient, the lower the boundary-layer Reynolds number at instability. In translating these results in terms of the blade-chord Reynolds number, the boundary-layer Reynolds number R_δ can be expressed as (Appendix V)

$$R_\delta = R_c[V_o/V_1](\delta/c) \qquad (3)$$

Thus the closer the point to the blade leading edge (the smaller the value of (δ/c), the larger the blade-chord Reynolds number (or V_o/V_1) necessary for the attainment of the instability value of the boundary-layer Reynolds number at that point. In other words, instability condition occur sooner at high blade-chord Reynolds numbers (or V_o/V_1). These considerations are illustrated graphically in figure 6, which shows the results of the calculation of the instability point for various blade-chord Reynolds numbers on

the surface of a Joukowski air foil at several angles of attack. The effect of the increased surface pressure gradient and Reynolds number on the location of the instability as angle of attack is increased is clearly indicated.

3.5 Effect of Free Stream Turbulence On Transition

The drag characteristics of spheres have provided a means for evaluating the effects of freestream turbulence on transition. As previously discussed, the instability theory has indicated that the critical Reynolds number at transition is a function of the turbulence parameter defined as $\beta(\ell^*/\nu)^{1/3}$ (Ref. 5). Experimental verification of this effect is represented by figure 8, which illustrated the earlier transition associated with increasing free-stream turbulence. The turbulence in a cascade tunnel is frequently expressed in terms of a turbulence factor, defined as the ratio of the critical Reynolds number

at zero turbulence to the measured critical Reynolds number of the sphere. The effective Reynolds number for a blade section, defined as blade-chord Reynolds number times turbulence factor of the tunnel has used to represent a transition parameter that includes the effects of free-stream turbulence.

3.6 Reynolds Number Effects on the Boundary Layer Momentum Thickness

Generally speaking, the boundary layer behavior is fairly well understood as long as the transition occurs either before the separation point or at a large distance downstream of the separation. In the former case a thickening of the boundary layer occurs in the region of transition as the flow passes to the turbulent state. In the latter case the laminar boundary layer remains separated, and the flow breakaway and high form drag are observed. When transition occurs close behind the point of laminar separation, however, under normal conditions, the separated laminar boundary may reattach to the surface as a turbulent layer, forming a sort of bubble of locally separated flow. The reattached turbulent boundary layer is considerably thicker than if transition had occurred at that point without a previous laminar separation.

Attempt is now made to construct a quantitative picture of the anticipated variation of boundary-layer momentum thickness on a blade surface over a wide range of Reynolds number, pressure distribution, and turbulence level. Such a composite plot will not only constitute an effective summary of the preceding theory as applied to blade sections, but may also be of interest in identifying desirable or undesirable areas of cascade operation.

The comparative variation of trailing-edge boundary-layer momentum thickness (θ/c) with blade-chord Reynolds number is presented for two levels of pressure gradient in figure 9 (data obtained from table 1, Chapter ϵ). At low values of Rc the boundary is entirely laminar, and θ/c decreases with increasing Rc as shown by curve d-c in accordance with the .5 power law. At some value of Rc, indicated by 'A' in the figure, Rc becomes sufficiently large that transition from a laminar to a turbulent layer occurs at the trailing edge. This Reynolds number appears to yield the minimum boundary-layer thickness. When the blade loading (lift coefficient) is increased, the transition moves forward from the trailing edge, and the boundary-layer thickness falls somewhere below the laminar and turbulent curves. Finally, as the transition point approaches the leading edge the boundary layer will essentially assume the characteristics of the fully turbulent flow.

The effect of increased turbulence level will cause the boundary layer transition phenomena to occur at lower values of Reynolds number and will therefore have the effect of shifting

point 'A' further to the left of curve c-c'. Increased turbulence will result in increasing the minimum boundary layer momentum thickness as shown in figure 9. However, the effect of turbulence vanishes when low Reynolds number is encountered. In this case, curve c-c coincides with curve c-c' and the flow resumes the laminar characteristics.

4.0 SUMMARY AND CONCLUDING REMARKS

4.1 Summary

The previous considerations indicate that a considerable range of trailing-edge boundary-layer momentum thickness can be obtained from blade sections, depending on the surface pressure distribution, Reynolds number, and turbulence level. In two-dimensional-cascade research, therefore, it appears highly desirable to identify the range of operation of the blade sections in the general loss against Reynolds number spectrum. Actually, the effective Reynolds number should be considered so that turbulence level can also be included. Such identification can aid in determining the best regions of cascade operation and also be of use in correlating test data from different compressor geometry. Furthermore, in view of the possible pronounced effect of the laminar breakaway at low Reynolds number, the question of Reynolds number effects might be a significant consideration in compressor design. Reduced Reynolds

number in compressor design may arise for small-scale model units and/or for operation at high altitude.

4.2 Concluding Remarks

It is apparent from the preceding analysis that the boundary-layer theory currently available is incapable of completely predicting the viscous flow about a two-dimensional cascade. However, the qualitative information provided by the theory can serve as a useful guide in obtaining and interpreting cascade data. Furthermore, some quantitative results can be obtained from the theory in its present state for a limited range of flow conditions and assumptions.

The principal conclusion reached from the qualitative evaluation of cascade boundary-layer behavior is the large sensitivity of the losses to blade-chord Reynolds number and free-stream turbulence. Apparently, a wide range of boundary-layer loss (in terms of θ/c) can be obtained for a conventional cascade geometry, depending upon Reynolds number and turbulence. The importance of the identification and evaluation of Reynolds number effects in cascade operation and data analysis is thereby indicated.

The primary shortcoming of quantitative evaluation is the inability of theory to predict the location and characteristics of the transition from laminar to turbulent flow. Widespread use of the quantitative calculations will follow the ability to locate the transition point successfully. This problem is difficult to be treated theoretically, an attempt should be made to determine an empirical correlation valid for the limited variety of blade shapes currently in use.

5.0 SOME DESIGN CONSIDERATIONS ON REYNOLDS NUMBER EFFECTS

It is now possible to establish some sort of design criteria with regard to the laminar breakaway and transition at low Reynolds number. At high positive incidences the pressure distributions have, on the convex suction surface, a sharp suction peak located close behind the leading edge. As the incidence is reduced this peak becomes more rounded and moves back towards the trailing edge. If the peak is too sharp and is followed by an excessively steep pressure gradient then the performance of the compressor will deteriorate significantly due to the pronounced viscous effect and the wake mixing behind the point of separation. Thus it appears that pressure distributions with a moderately

sharp suction peak near the leading edge on the convex surface are likely to give the best overall performance at low Reynolds number.

An appreciable pressure rise before the separation point will be beneficial in that it will promote early transitions and so tend to create a turbulent layer before the theoretical laminar separation point is reached. The type of pressure distribution which permits an appreciable pressure rise before the laminar separation point is of the form having a sharp suction peak close to the leading edge. Although the moderately peaked pressure distributions resulting from positive incidence angles give better characteristics at low Reynolds numbers by inducing transition to occur before the point of laminar separation. There is a definite limit to improvement by this means as above a critical incidence laminar breakaway is again encountered. For this reason and because the turbulent layer covers a large proportion of the surface due to early transition, losses in the turbulent region are increased. The advantage of designing for early transition to avoid laminar separation at low Reynolds numbers would be partly offset by the increased skin-friction drag at high Reynolds number.
It appears from equation (9) that there is an optimum blade-chord Reynolds number at which the maximum efficiency

is obtained. Although no theory has thus far given any indication of how this optimum Reynolds number can be determined, its existence has called for every consideration to be given in the preliminary design stage.

Although reliable design criteria for transition-point location for general airfoil flow are not currently available, some work has been done along these lines. An investigation of an NACA 65 series airfoil in reference 5 revealed that a criterion for transition based on boundary layer Reynolds number can be satisfactorily established as $R\delta = 800$ (where δ is the normal distance from the airfoil surface to a point within the boundary distance from the airfoil surface to a point within the boundary layer where the velocity is equal to 0.707 of the velocity at the outer edge of the boundary-layer). This result agrees closely with that of Donaldson (figure 7) and could be used as a design criterion to ensure improved performance over a large range of Reynolds number.

6.0 PREDICTION OF THE CRITICAL REYNOLDS NUMBER

A major difficulty yet remaining in the computation of blade boundary-layers is the successful prediction of the location of the transition point. This problem is in a very difficult realm of viscous-flow theory because of the close relation of the transition point to the Reynolds number and free-stream turbulence of the flow. From the previous analysis, it is shown that separation of laminar boundary occurs at the peak velocity point. The boundary layer must go into transitions so that a turbulent mechanism can be set to cause the flow to re-attach. As previously noted, transition is dependent upon Reynolds number (R_δ) calculated from boundary layer thickness and local velocity at a given point. Inspite of the fact that stream turbulence level and the pressure gradient influence this number considerably, some empirical correlations have found to exist between R_δ at separation and the length of the separated region. In principal, two distinct types of transition can take place; one holding for very low turbulence level (less than 1%) and the other occurring when the turbulence level is relatively high (say 3.4%).

In the case of turbomachine, high turbulence level is anticipated. The cascade data of Sawyer have now been used to construct the relation between the R_δ at separation and the length of the bubble as shown in fig. 10. (Ref.24 Two curves have been derived for turbulence levels of 1% and 3.4% respectively. By use of these experimental curves, the distance between the separation point and the point of reattachment can be estimated for any similar type of cascade if R_δ at separation is known. Furthermore, these curves can be used to find the case where the separation bubble will extend to the trailing edge of the airfoil, thus giving the critical Reynolds number.

The method is developed by combining the cascade data of fig. 10 and the theoretical results of Thwaites with regard to the boundary layer growth as follows: (Ref.5)

$$\theta^2 = .45\,\nu (V_s)^6 \int_0^s V_s^5\, ds \qquad \text{(10)}$$

and $$m = -\theta/\nu \, dV_s/ds \qquad \text{(11)}$$

(for separation $m = .082$)

In order to compute R_δ at the point of separation, it is necessary that both velocity distribution and blade chord Reynolds number are known.

Since $R_x = R_c V/V_\infty (S/C)$ ——— (12)

Assume that the curvature of the blade is small over the leading edge portion of the airfoil, the boundary layer thickness growth follows the form of a plate as expressed by equation (13). (Ref. 15)

$$\delta/S = 5/\sqrt{R_x} \quad \text{——— (13)}$$

where $R_x = V_\infty \delta/\nu = V_\infty C/\nu\,(\delta/C) = R_c \delta/C$ ——— (14)

$$\therefore \delta/S = 5/\sqrt{R_c}\sqrt{S/C} \quad \text{——— (15)}$$

This approximation is justified provided that the radius of curvature of the blade, R, is at least same order of magnitude as x. By writing the momentum equation in the direction normal to one surface as in ref. 29

$$\partial P/\partial y = [o]\rho V^2/R \qquad (16)$$

where y = position vector normal to the surface

R = curvature of the surface

[o] = "the order of magnitude of"

or $\Delta P|_{\text{boundary layer}} = [o]\rho V^2 \cdot y/R$

$= [o]\rho V^2 \delta/x \cdot x/R \quad (\because \delta \approx \Delta y)$

Now, if $\frac{x}{R}$ is of order of magnitude unity or less, it follows that $\Delta P|_{\text{boundary layer}}/\rho V^2$ is not greater

in order of magnitude than $(\frac{\delta}{x})$. This means that pressure within the boundary layer at any value of x scarcely differs from the pressure at the edge of the boundary layer at the same value of x. Thus, the approximate momentum equation in the y direction takes the trivial form

$$\frac{\partial P}{\partial y} = 0 \quad \left(\text{only if } \mathcal{R}_{x/\delta} \to \infty \right) \qquad (17)$$

Hence, for a flat plate:

$$\frac{\delta}{x} = \frac{5}{\sqrt{R_x}} \qquad (18)$$

It follows that

$$\frac{\delta}{c} = \frac{5}{c}\frac{\delta}{\sqrt{R_c}\sqrt{\delta/c}} = \frac{5}{\sqrt{R_c}}\sqrt{\frac{\delta}{c}} \qquad (19)$$

hence

$$R_\delta = R_c V_\delta / V_\infty \, (5/\sqrt{R_c})\sqrt{\delta/c}$$
$$= \sqrt{R_c}\, V_\delta / V_\infty \, 5\sqrt{\delta/c} \qquad (20)$$

The relation of $(\frac{V_\delta}{V_\infty})$ vs $(\frac{\delta}{c})$ at separation condition has been established from figure (6). R_δ can now be obtained from equation (20) for any desired level of blade chord Reynolds number.

Equation (10) can be rewritten in dimensionless form in terms of the blade chord, inlet velocity and blade-chord Reynolds number. -

$$R_c(\theta/c)^2 = .45(V_0/V_1)^{-6}\int_0^{x}(V_0/V_1)^5 d(x/c) \qquad (21)$$

using the relation of

$$\begin{aligned} R_\delta &= R_c V_0/V_1\ \delta/c\ \delta^*/\theta\ \delta/\delta^* \\ &= R_c V_0/V_1\ \theta/c\ \delta/\delta^* H \end{aligned} \qquad (22)$$

where $H = \delta^*/\theta$; $R_\delta = V_0\delta/\nu$

$$V/\nu = R_c V_0/V_1\ \theta/c\ \delta/\delta^* H$$

$$V_0 c/\nu = R_c V_0/V_1\ (\theta/c)(c/\delta^*) H$$

$$R_c = R_c V_0/V_1\ (\theta/c)\ c/\delta^* H$$

Finally

$$\delta/c = V_0/V_1\ (\theta/c)\ \delta/\delta^* H \qquad (23)$$

where $(\frac{\delta}{c})$ is a function of Reynolds number and the velocity distribution as expressed by equation (5b).

The quantity δ/δ^* in equation (23) can be evaluated from a typical boundary layer velocity distributions just prior to separation and can be assumed to be constant with Reynolds number. Alternatively, it is possible to approximate this quantity (δ/δ^*) using flat plate approach as follows:

Since $\delta/x = 5/\sqrt{R_x}$

and $\delta^*/x = 1.72/\sqrt{R_x}$

Thus, $\delta/\delta^* = \delta/x \cdot x/\delta^* = 5/1.72 = 2.9$ ——— (24)

The value of 'H' is generally taken as 2.5 when separation of the boundary layer is impending. (Ref.7)

λ, by definition, is the ratio of the length of the separated region to the boundary layer tickness δ at the point of separation.

Hence

$$\lambda = (C - S)/\delta$$

$$= \frac{1 - (S/C)}{\delta/C} \quad \text{——— (25)}$$

substituting (23) into (25), we have

$$\Lambda = \left[\frac{1-(\delta/c)}{H(V_1/V_1)\delta/\delta^*}\right]\frac{1}{(\theta/c)}$$

$$= \left[\frac{1-(\delta/c)}{7.3\,V_1/V_1}\right]\frac{1}{(\theta/c)} \qquad \text{(26)}$$

$$= A/(\theta/c)$$

where $A = \left[\frac{1-(\delta/c)}{7.3\,V_1/V_1}\right]$

Λ is computed as a function of R_δ at the range of critical Reynolds number in the following fashion. (Table 1)

TABLE 1. Calculation of Λ vs R_δ for various velocity distribution.

		Turbulence level = 3.4%				Turbulence level = 1%				
		$C_L = 1$		$C_L = 0$		$C_L = 1$		$C_L = 0$		Remarks
(1)	$(\frac{\delta}{c})$	.28	.28	.42	.42	.28	.28	.42	.42	figure 6
(2)	I	.0595	.0595	.0976	.0976	.0595	.0595	.0976	.0976	equation 5e
(3)	$\sqrt{I}$	.244	.244	.312	.312	.244	.244	.312	.312	from (2)
(4)	$(\frac{V_o}{V_1})$	1.68	1.68	1.3	1.3	1.68	1.68	1.3	1.3	figure 6
(5)	R_δ	10^3	$.6\times10^3$	$.8\times10^3$	$.6\times10^3$	$.74\times10^3$		$.8\times10^3$		select trial
(6)	$\sqrt{R_c}$	2.24×10^2	1.35×10^2	1.89×10^2	1.42×10^2	1.66×10^2		1.9×10^2		equation 20
(7)	R_c	$.502\times10^5$	$.182\times10^5$	$.358\times10^5$	$.205\times10^5$	$.276\times10^5$		$.362\times10^5$		from (6)
(8)	$(\frac{\vartheta}{c})$	1.09×10^{-3}	1.66×10^{-3}	1.65×10^{-3}	2.2×10^{-3}	1.47×10^{-3}		1.64×10^{-3}		equation 5b
(9)	A	.0585	.0585	.061	.061	.0585		.061		equation 26
(10)	Λ	53.5	35.2	37.0	27.7	40.0		37.2		

Another relation exists that must be satisfied at separation: namely, the experimental curve shown in fig. 10. Graphing these two relations simultaneously gives the critical Reynolds numbers (fig. 10).

By plotting the results of Table 1 in figure 11, we obtain a quantitative relation for turbulence level, velocity gradient and critical Reynolds number at transition. By reducing the turbulence level and velocity gradient (lift coefficient) the critical Reynolds number tends to go to a higher value. This means transition from laminar to turbulent is delayed in agreement with the previous qualitative analysis.

8.1 Concluding Remarks

However, the foregoing predicted critical Reynolds number is unique for each compressor configuration. The critical Reynolds number in fact varies from one geometric configuration to another. It is therefore a very difficult task to establish any one value of limiting Reynolds number that will hold for all blade shapes (the term limiting Reynolds number refers to the value of Reynolds number at which large rise in loss is observed). On the basis of

the available cascade data presented in figure 11, it appears that serious trouble in the minimum momentum thickness region may be encountered at blade-chord Reynolds numbers below $.6 \times 10^5$. (Ref.5)

It seems there exist a universal critical Reynolds number for compressors of different design which can be generalized in a fashion similar to the well-known critical Reynolds for pipe flow, provided that the compressors are of geometric similar, for example, a representative model scaled from a prototype. Although, some work has been done along this line in an attempt to generalize the flow parameters such as friction coefficient vs Reynolds number from one geometry to another (Ref. 17), the information on this subject investigation is by no means complete and is limited only to some simple geometries such as rectangular ducts and circular pipes. In addition, the flow correlations (Ref.17) between these geometries held only in a certain range of Reynolds number. It appears that there is a need to further this trend of study so that a more universal critical Reynolds can be generalized from the test results of cascade and compressors of different size and shape. This universal critical Reynolds number level is anticipated to have a value of $.6 \times 10^5$ based on the interpreted data.

7.0 THEORECTICAL ANALYSIS OF REYNOLDS NUMBER EFFECTS ON THE FLUID PROPERTIES

In order to derive the basic relationships between the fluid properties and the Reynolds Number, it is worthwhile to examine the energy exchange rate in the mean flow and the disturbances. Dr. Mollochristensen (Ref. 14) has recently developed the energy exchange equations from the equations of motion. For mean flow the energy equation is in the form of:

$$\frac{\partial E}{\partial t} = -U_j \partial(u_i u_j)/\partial x_j - \nu \frac{\partial u_i}{\partial x_j}\frac{\partial u_i}{\partial x_i} + \frac{\partial}{\partial x_i}\left[-P u_j/\rho + u_j E + \nu/2 \frac{\partial E}{\partial x_j}\right] \quad (27)$$

and for disturbance:

$$\frac{\partial \mathcal{E}}{\partial t} = -\left\{u_i u_j\right\}\frac{\partial u_i}{\partial x_j} - \nu\left\{\frac{\partial u_i}{\partial x_j}\frac{\partial u_i}{\partial x_j}\right\} + \frac{\partial}{\partial x_j}\left[-\left\{P u_j/\rho\right\} + u_j\left\{\mathcal{E}\right\} + \left\{u_j \mathcal{E}\right\} + \nu/2 \frac{\partial \mathcal{E}}{\partial x_j}\right] \quad (28)$$

The first two terms in the right of equation, (27 and 28) show that the fluctuations, through the Reynolds stresses, change 'E' (& ('$\mathcal{E}$')) and that 'E' (& ('$\mathcal{E}$')) also decay due to viscous dissipation. The third term of equation (27) and (28) can be regarded as divergence term. Thus integrating equation (27) over the volume defined by

the solid boundary to obtain the following relation:

$$\left(\frac{\partial}{\partial t}\right)\iiint \mathcal{E}\,dV = -\iiint u_i u_j \left(\frac{\partial u_i}{\partial x_j}\right) dV - \iiint D\,dV + \iint_s \left[-P u_j/\rho + u_j \tau_{ij} + \nu \frac{\partial \mathcal{E}}{\partial x_j}\right] dS \quad \text{---} \quad (29)$$

The surface integrand (third term) is zero since it vanishes on the boundary and in the free stream as well. We have, therefore,

$$\left(\frac{\partial}{\partial t}\right)\iiint \mathcal{E}\,dV = -\iiint \left(u_i u_j \left(\frac{\partial u_i}{\partial x_j}\right) + D\right) dV \quad \text{---} \quad (30)$$

To convert the above equations into a nondimensional form, we introduce a velocity scale U_o, and a length scale δ, such that

$$\left(\frac{\partial}{\partial t'}\right)\iiint \mathcal{E}'\,dV = -\iiint u_i' u_j' \left(\partial u_i'/\partial x_j'\right) dV - \left(1/R_\delta\right)\iiint D'\,dV \quad \text{---} \quad (31)$$

where, D = The product of viscous stress and strain

$$= \nu \frac{\partial u_i}{\partial x_j} \frac{\partial u_i}{\partial x_j}$$

= The dissipation function for fluctuations

$R_\delta = U_o \delta/\nu$ is the boundary Reynolds number

and the primes denote nondimensional variables.

As indicated by equation (31), the growth of instability is thus governed by a balance between production (first term) and dissipations (second term) of fluctuations. This balance is directly dependent upon Reynolds number. It becomes obvious that for each laminar flow there is a unique critical Reynolds number which marks the instability. When similarity is maintained in the region of laminar flow, the basic relation between the Reynolds number and fluid properties is of the form:

$$N^n \propto 1/R_s \quad \text{for laminar flow} \qquad (32)$$

where 'n' is to a large extent determined by empirical correlations.

Since Reynolds number is a measure of the largest scale (inertia force) to a viscous dominated scale (viscous force) with a given typical velocity, the ratio of large to viscous limit scales increases at high Reynolds number. Let λ_j be the wavelength of the jth instability; if similarity in the turbulent flow is assumed such that

$$\lambda_1/\lambda_2 = \lambda_2/\lambda_3 = \cdots = \lambda_{n-1}/\lambda_n = \alpha^{-1} \qquad (33)$$

we find $$\lambda_n/\lambda_1 = \alpha^N \qquad (34)$$

and $$N \propto \log \lambda_n/\lambda_1 \qquad (35)$$

taking λ_N/λ_1 to be a measure of the Reynolds number

$$N = n \log R_c \qquad \text{for turbulent flow} \text{ -------- (36)}$$

This means that large changes in Reynolds number is required to make significant changes in fluid properties. The value of 'n' is again to be determined from empirical correlation.

8.0 REYNOLDS NUMBER EFFECTS ON THE EFFICIENCY OF TURBOMACHINERY

The investigation on losses in cascades performed over the last decade and the refinements in boundary-layer theories have contributed significantly to the understanding of the nature of these losses. Only a certain percentage of the losses are viscous losses and the remainder of the losses is caused by separation of the boundary layer from the blade surface and subsequent mixing. The significance of these different types of losses with regard to Reynolds number effects is that only the viscous losses expressed by a friction coefficient, follows the usual Reynolds number relation, ie (Ref.2)

$$f = K R_c^{-n} \text{ ------ (37)}$$

$$\text{or } (1-\eta) = K_1 R_c^{-n} \text{ ------ (38)}$$

Where $n = 0.2$ to 0.25 for turbulent flow

and $n = 0.5$ for laminar flow.

In contrast, the separation and mixing losses do not necessarily follow equations (38) and may only be insignificantly affected by the Reynolds number.

Series of cascade test have been carried out in a number of institutes to determine the effects of Reynolds number on the performance of a compressor. Most of the early work was reviewed by Ainely with emphasis on the changes in efficiency. It has been reported by many investigators that the efficiency did in fact vary according to Re^{-n}. The value of 'n' appeared to be affected by compressor geometry and inlet Mach number level. (Ref.24)

Two definitions of efficiency have been used to calculate the performance of turbomachinery. The compressor overall efficiency η_c is defined in terms of the ratio of the work supplied per unit flow rate in a reversible adiabatic compressor to the actual work supply per unit flow rate in the actual compressor between similar entry and delivery pressure. Another concept of efficiency is often used, ie, the small stage polytropic efficiency, η_p which defines the

compression through a small increment of pressure. The relation between the polytropic efficiency and the overall efficiency may be obtained for a gas of constant specific heat. Reference 18 derives the desired relation as (Appendix III)

$$\eta_c = \left\{\left(P_1/P_1\right)^{\frac{\kappa-1}{\kappa}} - 1\right\} \Big/ \left\{\left(P_2/P_1\right)^{\frac{\kappa-1}{\kappa\eta_p}} - 1\right\} \qquad (39)$$

In general practice, the inefficiency (or loss) being defined as $(1 - \eta_p)$ is used for data correlation from which the value of 'n' is determined. As suggested by equation (32), the effects of Reynolds number on the inefficiencies can be generally correlated by the equation of the form (Ref. 24)

$$\frac{1-\eta_c}{1-\eta_{ref}} = A + (1-A)\left(R_c/R_{c\,ref}\right)^{-n} \qquad (40)$$

where 'A' represents the source of losses independent of Reynolds number. In order to concentrate on the effects of Reynolds number on the loss characteristics it appears convenient to set "A" = 0 resulting in the following expression

$$\frac{1-\eta_c}{1-\eta_{ref}} = \left(\frac{R_c}{R_{c\,ref}}\right)^{-n} \qquad (41)$$

where $n = p.q$ (42)

'p' and 'q ' are defined as the Mach number correlation parameter and compressor sensitivity parameter respectively. The correlation parameter 'p' has been established as shown in figure 12 by NACA method of estimating shock loss (Ref. 24) The parameter 'q' was correlated by combining the effects of aspect ratio and the geometry of a multi-stage compressor in such a way that the parameter 'q' represents a quantity being defined by the ratio of effective length to the mean annulus height. Figure 13 shows the influence of compressor geometry on compressor sensitivity to Reynolds number.

The value of 'n' has been reported to vary from .1 to .2 in the turbulent flow regime and reach .5 in the laminar flow regime. Some of the test data of a PT6 T400 gas turbine obtained by UACL is presented in figure 14. (Ref.29). The change in compressor efficiency has been found to follow the law of $(1 - \eta_p) = k\ Re^{-n}$ where the index 'n' has a value of .131 (slope = 7.60) above the critical Reynolds number. The value of 'n' is found in agreement with n = .104, using the n = p.q correlation.

One of the best reported tests (Ref. 4) on Reynolds number effect is also shown in figure 14. According to

these results, the value of $(1 - \eta_p)$ is inversely proportional to the .2 power of the Reynolds number through the range of Reynolds numbers above $.5 \times 10^5$ provided that the compressor passage is aerodynamically smooth. When the surfaces are rough, there will be no variation in performance with Reynolds number (ie, 'n' approaches zero). In this respect, the flow pattern through the compressor exhibits the same basic characteristics as other fluid flows. However, when the Reynolds number falls in the range of $.1 \times 10^5$ to $.5 \times 10^5$, the inefficiency is found inversely proportional to the .5 power ('n' = .5), indicating that the flow has entered the laminar flow regime. For the purpose of comparison, a summary of results suggested by Carter, et al is given below: (Ref. 23)

$$(1-\eta_p) = K_1 R_c^{-.2} \quad \text{for} \quad R_c \geq .5 \times 10^5 \qquad (43)$$

$$(1-\eta_p) = K R_c^{-.5} \quad \text{for} \quad R_c < .5 \times 10^5 \qquad (44)$$

In view of the fact that no evidence is given in the above literature to indicate which efficiency is quoted. It is believed that the correlation obtained by Carter, et al is based on the overall efficiency. To illustrate this point further, figure 15 shows the test results of a NASA compressor (Ref. 13) in which the overall efficiency is quoted and the .2 power law is observed. In order to show the difference when the definition of polytropic efficiency is used, the test results are replotted in

figure 14 using the relation of equation (37) for conversion. The result is that the index 'n' decreases to .1, when the polytropic efficiency is employed.

8.1 Concluding Remarks

It appears that the .1 and .2 power law tend to give a more accurate correlation when compressor performance is referred to polytropic efficiency and overall isentropic efficiency respectively. Theorectically, better performance may be achieved at very low Reynolds number by artificially agitating the boundary layer. This statement is based on the observation that some poor units at high Reynolds number provide slightly better performance at low Reynolds number. The importance of boundary layer development on the performance of compressor is thus recognized.

9.0 REYNOLDS NUMBER EFFECT ON COMPRESSOR TEMPERATURE RISE

Because the calibration of temperature probes varies with Reynolds number, it is extremely difficult to determine the effect of Reynolds number on compressor temperature rise.

The overall temperature rise is: (Ref. 12 &13)

$$\left.\frac{\Delta T}{T_1}\right|_{OVERALL} = \left.\frac{\Delta T}{T_1}\right|_{AERO} + \left.\frac{\Delta T}{T_1}\right|_{SHF.} \qquad (45)$$

where $\left.\frac{\Delta T}{T_1}\right|_{AERO}$ is also known as slip factor $\left(\frac{gJC_p\Delta T}{U^2}\right)_{AERO}$ which indicates the gas temperature rise due to energy additions. $\left.\frac{\Delta T}{T_1}\right|_{SHF}$ defines the windage factor $\left(\frac{gJC_p\Delta T}{U^2}\right)_{WINDAGE}$ which measures the gas temperature rise due to windage at the back face of the compressor and the casing as well. The compressor work factor is defined as the sum of slip factor and windage factor.

The change in $\left.\frac{\Delta T}{T_1}\right|_{SHF}$ with Reynolds number can be estimated by the law of friction factor on a flat plate resulting in the following expression:

$$\frac{\Delta T_{SHF1}}{\Delta T_{SHF2}} = \frac{f_2}{f_1} \qquad (46)$$

The windage factor is therefore considered to be a function of weight flow and Reynolds number. Reference 13 reveals

that the temperature rise due to windage, decreases linearly as flow rate increases. The variation of friction as a function of R_c is given below

$$f = 1.328\ (R_c)^{-.5} \quad \text{for laminar flow} \text{ ------ (47)}$$

$$f = .074\ (R_c)^{-.2} \quad \text{for turbulent flow} \text{ ----- (48)}$$

The observed trend in compressor work factor shows that the slip factor is also a function of flow rate and Reynolds number. If the relative flow angle leaving the trailing edge is assumed to be essentially constant (constant deviations), the slip factor will decrease linearly as the axial velocity is increased. Since decreasing Reynolds number tends to increase through flow velocity it should also decrease slip factor.

In summary, both components of work factor, ie, slip factor and windage factor should decrease with increasing flow. However, the slip factor should increase with increasing Reynolds number, while the windage factor should decrease.

Fig. 16 shows the compressor work factor vs design equivalent flow for different Reynolds number level at which the data were obtained. These data were gathered from the test results of a NASA 6" compressor (Ref. 17). It illustrated that the work factor is a function of equivalent weight flow and is practically independent of Reynolds number. From equation (45) it follows that

$$\left(\frac{\Delta T}{T_1}\right)_{OVERALL} = \text{constant regardless of Reynolds number variation.}$$

9.1 Concluding Remarks

This important result confirms the early observation in Chapter (2.0) that the shifting of compressor operating point due to variation in Reynolds number follows the constant $\frac{\Delta T}{T_1}$ line on the compressor map. It is also true to conclude that the compressor overall temperature rise is practically insensitive to any change in Reynolds

12.0 REYNOLDS NUMBER EFFECT ON MASS FLOW

The maximum mass flow passing through a compressor at any given speed will be determined by choking in one of its blade rows. It has been found, in general practice, that the flow is usually governed by choking in the first stage rotor when operated at or near design condition (design speed). This can be explained by the fact that the Mach number level is higher in rotors than stators and that it tends to fall throughout the machine due to increasing temperature. However, these conditions do not apply at low speeds and the flow is normally determined by the final stage. On this basis, the Reynolds number which will enable one compressor to be compared with another is one defining the flow conditions within the first rotor blade passage.

Comparison plots of total pressure ratio at design speed for seven levels of Reynolds number is presented in figure 17 as a function of design equivalent mass flow. These data are obtained from the test results of a NASA 6-inch centrifugal compressor at design speed (Ref. 13). As the Reynolds number was decreased from one level to

another, the mass flow decreases accordingly. These trends can be explained in terms of the boundary layer thickness increasing with lower Reynolds number, thereby decreasing the effective flow areas throughout the compressor. The relations of mass flow vs Reynolds number can be developed based on the model law (Moody formula) as follows: (Ref. 16)

$$\frac{1-\eta_1}{1-\eta_2} = \left[\frac{D_1}{D_2}\right]^n \qquad (49)$$

This expression shows that the ratio of the losses in two machines is a function of the ratio of the linear dimensions of the machines compared.

Consider that D_1 and D_2 represent the dimensions of one machine including its boundary layer thickness at two different levels of Reynolds number. If the Mach number remains practically unchanged, such that the mass flow is proportional to the effective flow area (D^2) then,

$$\frac{\dot{m}_2}{\dot{m}_1} = \left(\frac{D_2}{D_1}\right)^2 \qquad (50)$$

since $$\frac{1-\eta_1}{1-\eta_2} = \left(\frac{R_{c2}}{R_{c1}}\right)^n \qquad (51)$$

$$\left(\frac{\dot{m}_2}{\dot{m}_1}\right)^{1/2} = \left(\frac{R_{c2}}{R_{c1}}\right)^n \qquad (52)$$

thus $$\frac{\dot{m}_2}{\dot{m}_1} = \left(\frac{R_{c2}}{R_{c1}}\right)^{2n} \qquad (53)$$

By plotting mass flow and Reynolds number on the logarithm coordinate, we obtain the diagram shown in figure 18. The straight line relationship indicates that the index (.2/n) has a value equal to the slope of this straight line.

Hence $\frac{.2}{n} = .0875 = \tan 5°$

$$\therefore \eta = 2.3 \qquad (54)$$

Finally we obtain

$$\frac{m_2}{m_1} = \left(\frac{R_{e2}}{R_{e1}}\right)^{.0875} \qquad (55)$$

which is similar in nature to equation (32).

To verify this correlation further, some test data obtained by A.B. Wassel (Ref.24) and UACL (Ref.29) have been replotted in figure 18. It was found that they also follow closely the same correlation as shown in equation (55). The difference of these straight lines is immaterial since they represent a geometry of their own. Nevertheless, this correlation is applicable to any turbomachinery provided that they are operating at or close to design speed with the exception that there is a variation in Reynolds number.

10.1 Concluding Remarks

The foregoing analysis does not restrict itself to two dimensional flow nor does it ignore the casing boundary layer effect. Since temperature rise ratio is insensitive to any change in Reynolds number, it is possible to define the locus of constant $\frac{\Delta T}{T_1}$ on the the compressor map simply by calculating the mass flow according to equation (55) at the corresponding Reynolds number. A typical constant $\frac{\Delta T}{T_1}$ locus is shown in figure 17.

11.0 REYNOLDS NUMBER EFFECT ON PRESSURE RATIO

In comparing efficiencies of differing overall pressure ratio, it is essential to compare their polytropic efficiencies (or infinitesimal stage efficiency). This efficiency assumes that actual pressure rise is achieved by an infinite number of small increasements in pressure at the same efficiency being therefore independent of pressure ratio. The polytropic efficiency η_p is calculated from the measured temperature rise and pressure according to the following expression:

$$\eta_p = \frac{(K-1)\ln(P_2/P_1)}{K \ln(T_2/T_1)} \qquad (56)$$

or $$\frac{T_2}{T_1} = \left(\frac{P_2}{P_1}\right)^{\frac{K-1}{K\eta_p}}$$

Since $\left(\frac{\Delta T}{T_1}\right)$ is independent of Reynolds number, we can write

$$\left(\frac{P_2}{P_1}\right)^{\frac{K-1}{K\eta_p}}\Bigg|_{REF} - 1 = \left(\frac{P_2}{P_1}\right)^{\frac{K-1}{K\eta_p}} - 1 \qquad (57)$$

$$\frac{1}{\eta_{p_{REF}}} \log\left(\frac{P_2}{P_1}\right)_{REF} = \frac{1}{\eta_p} \log\left(\frac{P_2}{P_1}\right) \qquad (58)$$

From equation (41), we have:

$$\frac{\eta_p}{\eta_{p_{REF}}} = \left(\frac{R_c}{R_{c\,REF}}\right)^n \qquad (59)$$

It follows that

$$\text{Log}(P_2/P_1) \Big/ \text{log}(P_2/P_1)_{REF} = \left[\frac{R_c}{R_{c_{REF}}}\right]^n \qquad (60)$$

$$\text{Log}(P_2/P_1) \propto R_c^n \qquad (61)$$

The appearance of logarithm in $(\frac{P2}{P1})$ indicates that the pressure ratio is more sensitive to change of Reynolds number than the efficiency or mass flow as discussed in the previous chapters. Again the index 'n' is to be determined from data correlation.

The performance of a 3.7 inch diameter six-stage NASA axial flow compressor (Ref. 12) and a 6-inch radial bladed centrifugal compressor (Ref. 13) are presented in Fig. 19 and 17 respectively. With these typical data being available, the method of determining the index 'n' is now summarized as follows:

(1) Select any constant $\frac{\Delta T}{T_1}$ line on a compressor map such as Fig. 17, except those being close to surge or choking conditions.

(2) Compute log $(\frac{P_2}{P_1})$ at the points of interception for each level of Reynolds number.

(3) Plot log $(\frac{P_2}{P_1})$ and the corresponding Reynolds number on the logarithm coordinates as shown in figure 20.

(4) Repeat (3) until enough points have been obtained and plotted in the above diagram.

(5) The index 'n' is now determined from the slope of the line joining all the points in figure 20.

With $n = \tan 4^{\circ} = .07$

The pressure ratio variation with Reynolds number is then formulated as follows:

$$\log (\frac{P_2}{P_1}) = KR_c^{.07} \qquad \text{---------- (62)}$$

11.1 Concluding Remarks

The performance degradation in pressure ratio appeared to be more sensitive to the change in Reynolds number than any other performance parameters.

12.0 CONCLUSIONS

The theoretical consideration of the boundary layer behavior and the analysis of test data lead to the following conclusions:

(1) The polytropic efficiency and the overall isentropic efficient compressor were found to follow the .1 and .2 power law in turbulent region respectively. The non-viscous losses are almost independent of Reynolds number variation.

(2) The Reynolds number effects on mass flow variations can be expressed as $M_2/M_1 = (Rc_2/Rc_1)^{.0875}$

(3) The performance degradation in pressure ratio appeared to be more sensitive to the change in Reynolds number than any other performance parameters. The correlation between the pressure ratio and Reynolds number can be expressed as

$$\log \left(\frac{P_2}{P_1}\right) = KR_c^{.07}$$

(4) The temperature $\frac{\Delta T}{T_1}$ has been proved theoretically and experimentally unchanged regardless of Reynolds number variation. The variation in compressor performance,

thus follows the constant $\frac{\Delta T}{T_1}$ line on the compressor map. Thus, a new compressor map can be predicted should there be a Reynolds number variation.

(5) Transition from laminar to turbulent flow is indicated by the critical Reynolds number which is in general a function pressure gradient distribution and the degree of turbulence in the main stream.

(6) The location and nature of transition point is extremely important in determining the performance of a compressor. Transition can be controlled by varying the blade-chord Reynolds number, and/or by the local velocity distribution in the free stream if the turbulence level has been fixed at a certain value.

(7) It is possible to predict and at the same time to locate the critical Reynolds number at which the transition takes place based on the combination of Thwaite's equation and the empirical cascade data provided that the compressor is geometrically similar.

(8) There is an optimum Reynolds number at which the maximum efficiency is obtained by balancing the losses between the laminar and turbulent region.

(9) The pressure distribution with a moderately sharp suction peak near the leading edge on the convex surface is likely to give the best overall performance at low Reynolds number.

(10) There is apparently a universal critical Reynolds number which can be generalized to apply to a family of compressor geometry. The method of correlation to enable more universal application of particular results is indicated.

(11) The Reynolds number effects could become significant on the performance of a turbomachinery when the laminar flow regime is predominating. The performance of a compressor can in fact deteriorate even more rapidly if separation of laminar layer has taken place before the point of transition.

(12) Based on the test data analysed, the Reynolds number effect on the performance of centrifugal units seem to be the same as that of axial flow type.

13.0 RECOMMENDATION

Further investigation on this subject study could include:

(1) Theorectical and/or empirical methods of determining the optimum and universal critical Reynolds number should be attempted.

(2) Theorectical methods could be used to derive the most suitable form of pressure distribution for a given Reynolds number. This pressure distribution is of useful in selecting the compressor geometry in its preliminary design stage.

(3) More work have to be doen in connection with transition problem so that reliable design criteria can be set forth for very general conditions of Reynolds number, turbulence and pressure distribution. When such criteria are available, theorectical boundary layer calculations will probably have to concern themselves with a range of possible transition point locations.

(4) There are still other sources of Reynolds number effects to be considered in the development of the casing boundary layer and in the case of three-dimensional flow. Also, the extent to which cascade viscous-flow characteristics will be reflected in the compressor is questionable. The answer to these questions must be supplied by continued comparative research.

14.0 REFERENCES

(1) "A computer study of an analytical model of boundary layer transition"
Coleman. Dup. Donaldson, AIAA Journal,
February 1969.

(2) "A study on Reynolds number effects in turbomachines"
O.E. Balje, Journal of Engineering for Power,
July 1964.

(3) "An Analysis of the performance of an axial flow compressor at low Reynolds number"
Robert Sohn, Journal of Aeronautical Science,
August 1956.

(4) "An analysis of Reynolds number and scale effects on performance of turbomachinery"
R.O. Bullock, Journal of Engineering for Power,
July 1964.

(5) "Aerodynamic design of axial flow compressor"
NASA Staff, Vols. I - III. N.A.C.A. R.M. E56B03, 1956.

(6) "Application of boundary layer theory in turbomachinery.
H. Schlichting, Journal of basic engineering,
December 1959.

(7) "Axial subsonic compressor design", S. Tou, ME711.1
Report, Sir George Williams University, 1972.

(8) "Axial flow compressor", Horlock, Butterworths,
Scientific Publications, 1958.

(9) "Approximate calculation of the laminar boundary layer"
B. Thwaites, Aero. Quart., Vol. 1,
November 1949.

(10) "Boundary layer theory", H. Schlichting, transl.
J. Kestin. McGraw-Hill, New York, 1960.

(11) "Effect of Reynolds number on overall performance of a 3.7 inch-diameter six-stage axial flow compressor"
L.J. Heidelberg and C.L. Ball, NASA TN D-6628,
February 1972.

(12) "Effect of Reynolds number on overall performance of a 6-inch radial bladed centrifugal compressor"
L.J. Heidelberg and C.L. Ball, NASA TN D-5761,
April 1970.

(13) "Effects of Reynolds number on the flow of air through a cascade of compressor blades"
H.G. Rhoden, Cambridge University R&M 2919, June 1952.

(14) "Elements of fluid Mechanics", D.G. Shepherd
Brace and World, Inc. 1965.

(15) "Fluid mechanics of turbomachinery"
Wislicenus, Volume 1 & 2, Dover Publications Inc. 1965.

(16) "Fluid flow and energy losses in non-circular conduits"
D.J. Gunn and C.W. Darling, Trans. Instn. Chem. Engrs., Vol. 41, 1963.

(17) "Introduction to gas turbine", D.G. Shepherd,
Constable and Company Ltd. 2nd edition, 1960.

(18) "Lecture notes on gas turbine principles and practice"
Morris, United Aircraft of Canada Ltd. 1968.

(19) "Lecture notes on turbomachinery"
P.G. Hill, Queen's University, 1972.

(20) "Low Reynolds number experiments in an axial flow turbomachine"
J. Neustein, Journal of Engineering for Power, July 1964.

(21) "Physics of turbulent flow"
Erik-Mollo-Christensen, AIAA Journal, July 1971.

(22) "Reynolds number effects in cascades and axial flow compressors"
J.H. Horlock, R. Shaw, D. Pollard, and A. Lewkowicz, Journal of Engineering for Power, July 1964.

(23) "Reynolds number effect on axial compressor"
A.B. Wassel, Journal of Engineering for Power, April 1968.

(24) "Some comments on Reynolds number"
L.H. Smith, Jr., Journal of Engineering for Power, July 1964.

(25) "Study of NASA and NACA single-stage axial flow turbine performance as related to Reynolds number and geometry"
D.E. Holeski and W.L. Stewart, Journal of Engineering for Power, July 1964.

(26) "Small turbomachinery compressor and fan aerodynamics"
R.C. Pampreen, Journal of Engineering for Power,
July 1973.

(27) "Surge margin consideration in gas turbine centrifugal compressor"
Colin Rodgers, G.T.I. July-August 1972.

(28) "T400 Altitude Tests program with engine 604 N.A.P.T.C"
R. Toogood, United Aircraft of Canada Ltd.,
April 6 - July 9, 1970.

(29) "The dynamics and thermodynamics of compressible fluid flow"
Shapiro, Volume 1 & 2, Ronald Press, New York, 1958.

(30) "Thermofluid Dynamics", A.J. Reynolds,
Wiley-interscience. 1967.

APPENDIX I

Dimensional Analysis for the Compressible Flow Machine

The most common systematic approach to finding the dimensionless number from a set of independent variables is the method of Buckingham, often referred to as Π theorem or Buckingham's Π theorem. For the compressible flow machine analysis, we have the following significant variables which can be expressed conveniently in the form of:

$$Po_2, \eta = f(D, \text{Design}, Po_1, To_1, \dot{m}, U, \nu, R, k)$$

Where Po_2 and η are the pressure rise after compression and thermal efficiency respectively. They are treated as dependent variables.

D and Design represent the linear dimension and a particular design of the machine being tested.

Po_1 (inlet total pressure), To_1 (inlet total temperature) $\dot{m}$ (mass flow) and U (the mechanical rotational speed of the machine) are the basic parameters in test conditions.

ν (Kinematic Viscosity), R(gas constant) and k(specific heat ratio) represent the fluid properties.

Thus, a total of nine independent variables are present.

Since a consistent dimensional system is one that composed of the smallest number of quantities in terms of which all entities and relations can be expressed, we have in the case of turbo-machine fluid mechanics, such four 'prime' quantities as length (L) Mass (M), time (T) and temperature (θ). Therefore, according to the π theorem, we should have the following results.

9 (independent variables) - 4 (prime parameters)
= 5 (independent dimensionless groups)

Now each independent variable is written in the form in which only the prime parameters are present as follows:

Variables	Basic Dimensional Forms
D	L
Po_1	M/LT^2
To_1	θ
$\dot{m}$	M/T
U	$1/_2T$
ν	L^2/T
R	$L^2/\theta T^2$
k	—
Design	—

Mathematically, the first dimensionless group, π_1, can be found by chosing D, Po_1, To_1, R and $\dot{m}$ in the following fashion:

$$\pi_1 = D^a \, Po_1^{\,b} \, To_1^{\,c} \, R^d \, \dot{m}^e$$

$$L^0 * \theta^0 * L^0 * T^0 = L^a * (M/(L*T))^b * \theta^c * (L/(\theta*T))^d * (M/T)^e$$

$$= L^{a-b+2d} * M^{b+c} * T^{-2b-2d-e} * \theta^{c-d}$$

Hence
$$\begin{cases} a-b+2d = 0 \\ b+e = 0 \\ -2b-2d-e = 0 \\ c-d = 0 \end{cases}$$

With five variables and only four equations available, we can set e=1

then $b = -1$

$a+1+2d = 0$

$d = 0$

$d = 1/2$

$c = 1/2$

and $a = -2$

$$\begin{cases} a = -2 \\ b = -1 \\ c = 1/2 \end{cases}$$

$$\begin{cases} d = 1/2 \\ e = 1 \end{cases}$$

$$\therefore \Pi_1 = \frac{\dot{m}\sqrt{RTo_1}}{P\phi_1 D^2} = \text{The flow coefficient}$$

Similarly, we can find the second dimensionless group Π_2.

$$\Pi_2 = {}^{a}D^{b}R^{c}To_1^{d}$$

$$= T^{-a-2c}\, L^{b+2C}\, \theta^{d-c}$$

$$-a-2c = 0$$

$$b+2C = 0$$

$$d-c = 0$$

set $b = 1$

then $c = 1/2$

and $d = -1/2$

$a = 1$

Hence $\Pi_2 = \frac{DU}{\sqrt{RTo_1}}$ = the aerodynamic speed or the rotor Mach number

And $\Pi_3 = U^{a}D^{b}\nu^{c}$

$$= T^{-a-c}L^{b+2c}$$

$$-a-c = 0$$

$$b+2c = 0$$

set $a = 1$

then $c = -1$

and $b = 2$

$\Pi_3 = UD^2/\nu$ = Reynolds Number

$\Pi_4 = K$ = specific heat ratio

Π_5 = Design of the Machine.

Finally, we arrive in the form as follows:

$$Po_2/Po_1,\ \eta = f\left(\frac{\dot{m}\sqrt{RTo_1}}{Po_1 D^2},\ \frac{UD}{\sqrt{RTo_1 K}},\ UD^2/\nu\ ,\ \text{Design}, K\right)$$

Now for a given fluid and a particular machine K , R and Design are known quantities and we can reduce the above relation to

$$Po_2/Po_1,\ \eta = f\left(\frac{\dot{m}\sqrt{To_1}}{Po_1 D^2},\ \frac{UD}{\sqrt{To_1}},\ UD^2/\nu\right)$$

Therefore the performance of a machine is a function of flow coefficient, rotor Mach number and the Reynolds number as shown in figure 1.

Note however that another dimensionless group, the power coefficient can be constructed from the pressure ratio Po_2/Po_1 and the flow coefficient.

$$Po_2/Po_1 \times \frac{\dot{m}\sqrt{RTo_1}}{Po_1 D^2} = \frac{\dot{m}\, Po_2\, RTo_1}{\rho_{o1} D^2 \rho_{o1}\sqrt{RTo_1}}$$

$$= \frac{\Delta H}{\rho D^2 \rho_{o1}\sqrt{RTo_1}}$$

$$= \frac{\text{Power}}{D^2 Po_1 \sqrt{RTo_1}}$$

which is treated as a dependent dimensionless group.

APPENDIX II

Energy Conversion

Conversion of kinetic energy of compressible fluid to thermal energy.

The velocity components of a fluid particle is shown on a cylindrical coordinate; $\bar{C}_r$ represents the velocity component in the radial direction, $\bar{C}_\theta$, the velocity component in the tangential direction, and $\bar{C}_z$, the velocity in the axial direction.

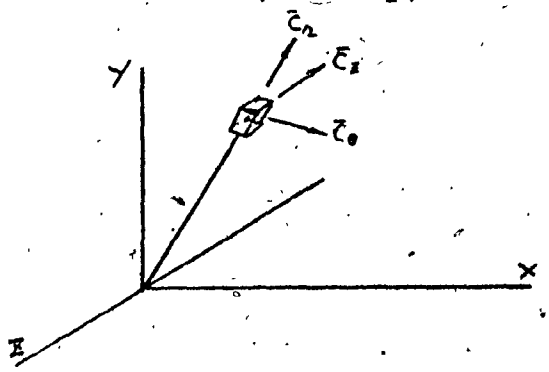

dm = the mass of the fluid particle.

gc=the acceleration of gravity.

$\bar{N}$=unit vector

Since $\bar{C} = \bar{C}_r + \bar{C}_\theta + \bar{C}_z$

and $\bar{F} = dm \frac{d\bar{C}}{dt}$

or $\bar{C} = \bar{N}_r C_r + \bar{N}_\theta C_\theta + \bar{N}_z C_z$

$\bar{F} = \bar{N}_r F_r + \bar{N}_\theta F_\theta + \bar{N}_z F_z$

But $\frac{d\bar{C}}{dt} = \bar{N}_r \frac{dC_r}{dt} + \bar{N}_\theta \frac{dC_\theta}{dt} + \bar{N}_z \frac{dC_z}{dt} + C_r \frac{d\bar{N}_r}{dt} + C_\theta \frac{d\bar{N}_\theta}{dt}$

$d\bar{n}_r = \bar{N}_\theta (d\theta \times 1)$

$\frac{d\bar{n}_r}{dt} = \bar{N}_\theta \frac{d\theta}{dt}$

and $\frac{d\bar{n}_\theta}{dt} = -\bar{N}_r \frac{d\theta}{dt}$

$\therefore \frac{d\bar{C}}{dt} = \bar{N}_r (\frac{dC_r}{dt} - \frac{d\theta}{dt} C_\theta) + \bar{N}_\theta (\frac{dC_\theta}{dt} + C_r \frac{d\theta}{dt}) + \bar{N}_z \frac{dC_z}{dt}$

Now $F_\theta = \frac{dm}{gc} a_\theta = \frac{dm}{gc} \left(\frac{dC_\theta}{dt} + C_R \frac{d\theta}{dt}\right)$

$$R F_\theta = dm \left(R \frac{dC_\theta}{dt} + R \frac{dR}{dt} \frac{d\theta}{dt}\right)/gc$$

$$= dm \left(R \frac{dC_\theta}{dt} + \frac{dR}{dt} C_\theta\right)/gc$$

$$= dm \frac{d}{dt} \left(\bar{R} \times \bar{C}\right)/gc$$

$R F_\theta$ = T = Torque applied to a fluid particle about the Z axis.

$\bar{R} \times \bar{C}$ = angular momentum about the Z axis

$$T = \frac{dm}{dt} d \left(\bar{R} \times \bar{C}\right)/gc$$

For steady, one dimensional flow, we can integrate over a control volume to obtain

$$\Sigma T = \Sigma \frac{dm}{dt} d \left(\bar{R} \times \bar{C}\right)/gc$$

$$\Sigma T = \frac{\dot{m}}{gc} \cdot d \left(\bar{R} \times \bar{C}\right)$$

$$= \frac{m}{gc} \left(R_2 C_{\theta_2} - R_1 C_{\theta_1}\right)$$

For axial flow compressor $R_2 = R_1 = R$

$$\Sigma T = \dot{m} R \left(C_{\theta_2} - C_{\theta_1}\right)/gc$$

$$W \Sigma T = \dot{m} W R \left(C_{\theta_2} - C_{\theta_1}\right)/gc \qquad \text{(W=rotational speed)}$$

$$\Delta H = \dot{m} U \left(C_{\theta_2} - C_{\theta_1}\right)/gc$$

$$\frac{\Delta H}{\dot{m}} = U \frac{\Delta C_\theta}{gc}$$

$$\Delta h = U \frac{\Delta C_\theta}{g_c} = C_p \Delta T \quad \text{——(1)}$$

Thus, the work(or temperature rise)per unit mass is equal to the product of rotational speed and the change in tangential velocity components.

Furthermore $\frac{\Delta h}{T_{01}} = \left(\frac{U}{\sqrt{T_{01}}}\right)\left(\frac{\Delta C_\theta}{\sqrt{T_{01}} g_c}\right) = \frac{C_p \Delta T}{T_{01}}$ ——(2)

The velocity triangle is shown at the mean section of a compressor rotor as follows:

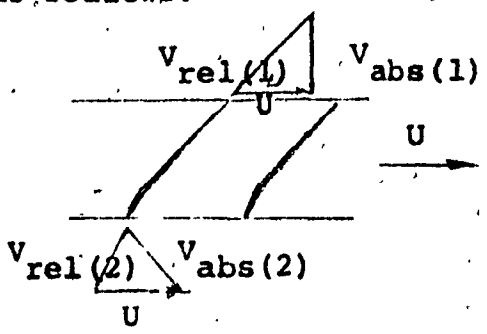

Abs = Absolute Velocity

rel = Relative Velocity

1 = inlet

2 = outlet

U =rotational speed

For the sack of illustration, the inlet velocity triangle is now combined with the outlet velocity triangle.

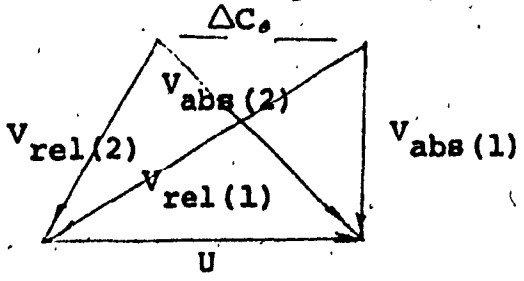

As indicated in equation (2) above, the velocity triangle is a function of inlet temperature (T_{01}). The above velocity diagram can be reconstructed to exclude the effect of inlet temperature variations without changing its shape.

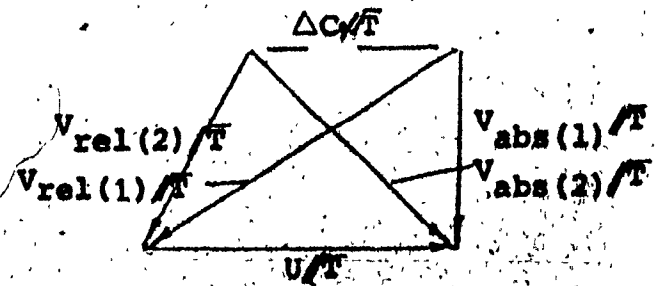

Now if $\frac{U}{\sqrt{T_{01}}}$ (rotor Mach Number) is kept constant $\frac{\Delta C_\theta}{\sqrt{T_{01}}}$ will remain unchanged in order that $(\frac{U}{\sqrt{T_{01}}})$ $(\frac{\Delta C_\theta}{\sqrt{T_{01}}})$ = Constant, and hence

$\frac{\Delta T}{T_{01}}$ = Constant.

This means the velocity diagram will not vary regardless of change in inlet conditions and hence eliminates the interference of one stage relative to the next. This results in only two independent variables of interest remaining in affecting the performance of a compressor. Equation (1) in Appendix I takes on the form of the following:

$$\frac{P_{12}}{P_{01}}, \eta = f\left(\frac{\dot{m}\sqrt{T_{01}}}{P_{01}} , \frac{V_D}{U} \right)$$

$$= f(\text{flow coefficient , Reynolds number})$$

APPENDIX III

Definition of Efficiency

(1) Over-all Isentropic Efficiency

The compression process can be demonstrated clearly on a temperature - entropy diagram as shown. The isentropic efficiency is defined as the ratio of ideal work to the actual work required to achieve the pressure rise. Hence we have,

$$\eta_c = \frac{\Delta h \text{ ideal}}{\Delta h \text{ actual}}$$

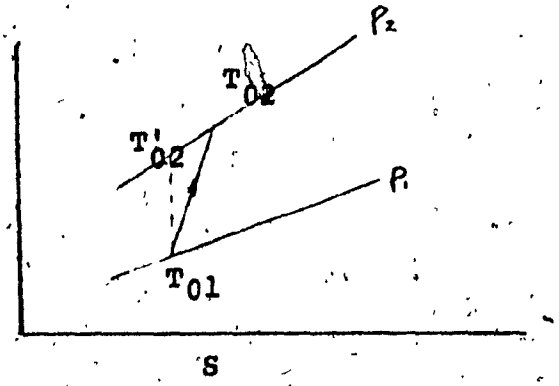

for ideal gas $h = C_pT$

Thus, $$\eta_c = \frac{C_p(T'_{02}-T_{01})}{C_p(T_{02}-T_{01})}$$

$$= ((T'_{02}/T_{01})-1)*T_{01}/\Delta T_0$$

Since $$T'_{02}/T_{01} = (P_{02}/P_{01})^{\frac{k-1}{k}}$$

Therefore, $$T_{01}((P_{02}/P_{01})^{\frac{k-1}{k}} -1)/\Delta T_0 \qquad (1.1)$$

(2) Polytropic Efficiency (or Infinitesimal Stage Efficiency)

When compression is accomplished with several similar stages of equal efficiency, the temperature at entry to each succeeding stage is higher than that due to isentropic compression by virtue of the inefficiency of the preceeding stage. This leads to the idea that there is an infinitesimal stage efficiency which is independent of pressure ratio or number of actual stages. Thus, for a small increment of pressure ΔP, from an initial pressure P, there is an isentropic efficiency η_P equal to $\Delta T/\Delta T'$. Thus, following the expression of equation (1.1) for a finite temperature change,

$$\Delta T' = T^* \left(\left(\frac{P+\Delta P}{P} \right)^{\frac{k-1}{k}} - 1 \right) / \eta_P$$

and $$\eta_P \Delta T'/T = (1+\Delta P/P)^{\frac{k-1}{k}} - 1$$

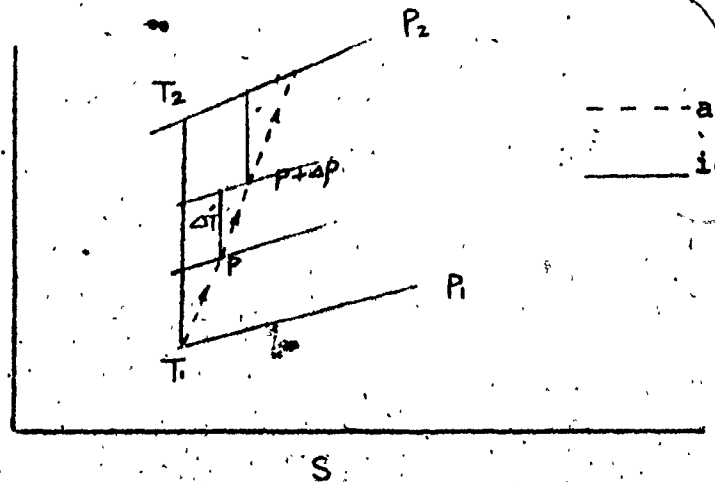

- - - - actual compression

_____ ideal compression

Expanding the term in brackets and dropping second order terms,

$$\eta_P \frac{\Delta T'}{T} = \left(1 + \left(\frac{K-1}{K}\right)\frac{\Delta P}{P}\right) - 1$$

$$= \left(\frac{K-1}{K}\right)\frac{\Delta P}{P}$$

and

$$\frac{\Delta T'}{T} = \left(\frac{K-1}{K\eta_P}\right)\frac{\Delta P}{P}$$

Replacing $\Delta T'$ with dT' and ΔP with dP and integrating over a finite pressure change P_1 to P_2 and temperature change T_1 to T_2

$$\int_{T_1}^{T_2} \frac{dT}{T} = \left(\frac{K-1}{K\eta_P}\right)\int_{P_1}^{P_2} \frac{dP}{P}$$

Hence

$$\ln\left(\frac{T_2}{T_1}\right) = \frac{K-1}{K\eta_P} \ln\left(\frac{P_2}{P_1}\right) \qquad (2.1)$$

and

$$\eta_P = \frac{\frac{K-1}{K}\ln\left(\frac{P_2}{P_1}\right)}{\ln\left(\frac{T_2}{T_1}\right)} \qquad (2.2)$$

Equation (2.2) gives and expression for η_P through a pressure ratio P_2/P_1 if the initial temperature T_1 and actual temperature for an irreversible process, T_2 are known.

(3) Conversion Expression for the Isentropic and Polytropic Efficiency.

From equation (2.1), a relationship between the infinitesimal stage efficiency η_P and the overall isentropic efficiency, η_c can be obtained. Equation (2.1) yields, after taking the anti-logarithm of both sides,

$$\frac{T_2}{T_1} = \left(\frac{P_2}{P_1}\right)^{\frac{K-1}{K\eta_P}}$$

from which

$$T_2 - T_1 = T_1\left(\left(\frac{P_2}{P_1}\right)^{\frac{K-1}{K\eta_P}} - 1\right) \qquad (3.1)$$

Now for the corresponding compression, the overall efficiency is η_c and

$$T_2 - T_1 = \frac{T_1}{\eta_c}\left(\left(\frac{P_2}{P_1}\right)^{\frac{K-1}{K}} - 1\right) \qquad (3.2)$$

Equating (3.2) and (3.1), then

$$\eta_c = \frac{(P_2/P_1)^{\frac{K-1}{K}} - 1}{(P_2/P_1)^{\frac{K-1}{K\eta_P}} - 1} \qquad (3.3)$$

Equations (3.3) allows η_c and η_p to be expressed in terms of pressure ratio.

Appendix IV

Reynolds Number Effects on the Flow Phenomena for which the Turbulent Level and Pressure Gradient along the Blade Surface are assumed to be Unvaried.

Figure 1 shows the flow condition at which the Reynolds number is so high that ($>10^6$) transition flow is promoted to occur before the laminar boundary separation point is reached. Turbulent flow is set up after the transition point.

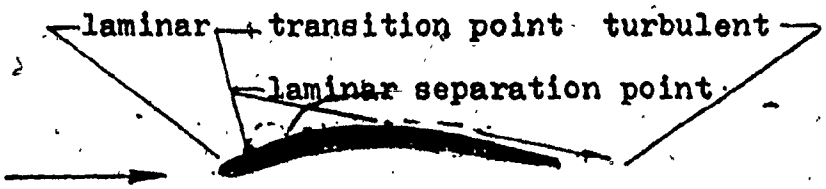

Fig.1flow through a cascade at high Reynolds NO.

As the Reynolds number is decreasing, the transition point moves toward the blade trailing edge as shown in figure 2. Turbulent flow is delayed. The reynolds number at which the transition point coincides with the separation point is called the critical Reynolds number. Under normal conditions, the turbulent boundary layer is able to reattach onto the blade surface. This turbulent boundary layer can tolerate a greater pressure gradient before the separation of turbulent boundary layer.

Fig.2 ortical Reynolds number

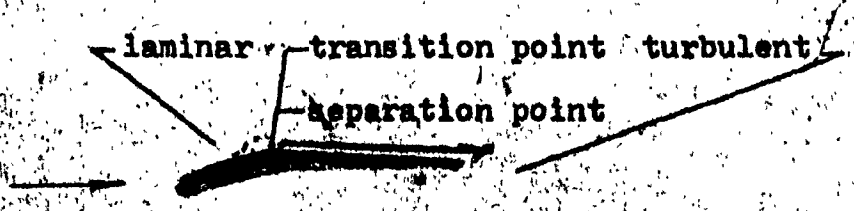

If the Reynolds number is further reduced, the laminar boundary layer will separate at the point of separation resulting in high pressure losses. This separated flow may be so stable that reattachment of the boundary layer is impossible.

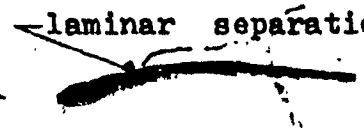

separation of laminar boundary layer at low Reynolds number.

Appendix V

Some Important Definitions

(1) Blade-Chord Reynolds Number

The flow of a viscous fluid near a solid surface is found to be dependent on the ratio of inertia to viscous forces. This non-dimensional ratio is called the Reynolds Number and is given by

$$Re = \frac{VD}{\nu}$$

The blade-Chord Reynolds Number is defined when the characteristic length D is based on the blade chord length C, hence $R_C = \frac{V_1 C}{\nu}$.

(2) Boundary Layer Reynolds Number

It is defined when the characteristic length D is based on the normal distance from the blade suction surface to a point within the boundary layer where the velocity is equal to .707 of the main stream.

$$R_\delta = \frac{V_0 \delta}{\nu}$$

$$= R_c \left(\frac{\nu}{V_1 C}\right)\left(\frac{V_0 \delta}{\nu}\right)$$

$$= R_c \left(\frac{V_0}{V_1}\right)\left(\frac{\delta}{C}\right)$$

(3) Suction Surface & Pressure Surface

A conventional blade section is shown

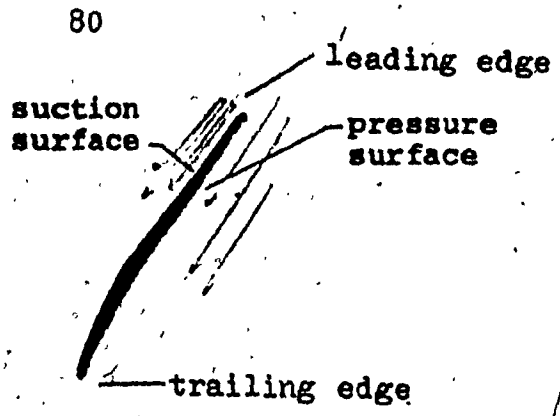

The convex surface tends to accelerate the flow and is called the suction surface; the concave surface tends to slow down the flow and is therefore called the pressure surface.

(4) Total drag and Lift Force

The force on a body that results from the motion of the body through a real fluid is, in general, inclined to the path direction. The component of this force parallel to the path is called the drag and the normal component is called the lift.

The total drag is the resultant of viscous drag(skin-friction drag) and pressure drag(form drag).

Skin-friction drag—The drag arising from the resolved components of the tangential stresses on the surface of the body. The effect of these components, taken over the whole exposed surface of the body, is the surface friction drag.

Pressure drag—It is defined as the drag forces arising from the resolved components of the normal pressure on the boundary under consideration.

Appendix VI

Relation of Lift, Drag and Loss Coefficient of a Two-dimensional Cascade and Their relations with Reynolds Number. (Ref. 8&29)

(For definition of lift, drag and losses refer to Appendix V)

The axial force (F_x) exerted by the fluid on each blade in the direction shown in the sketch below is determined from the momentum equation

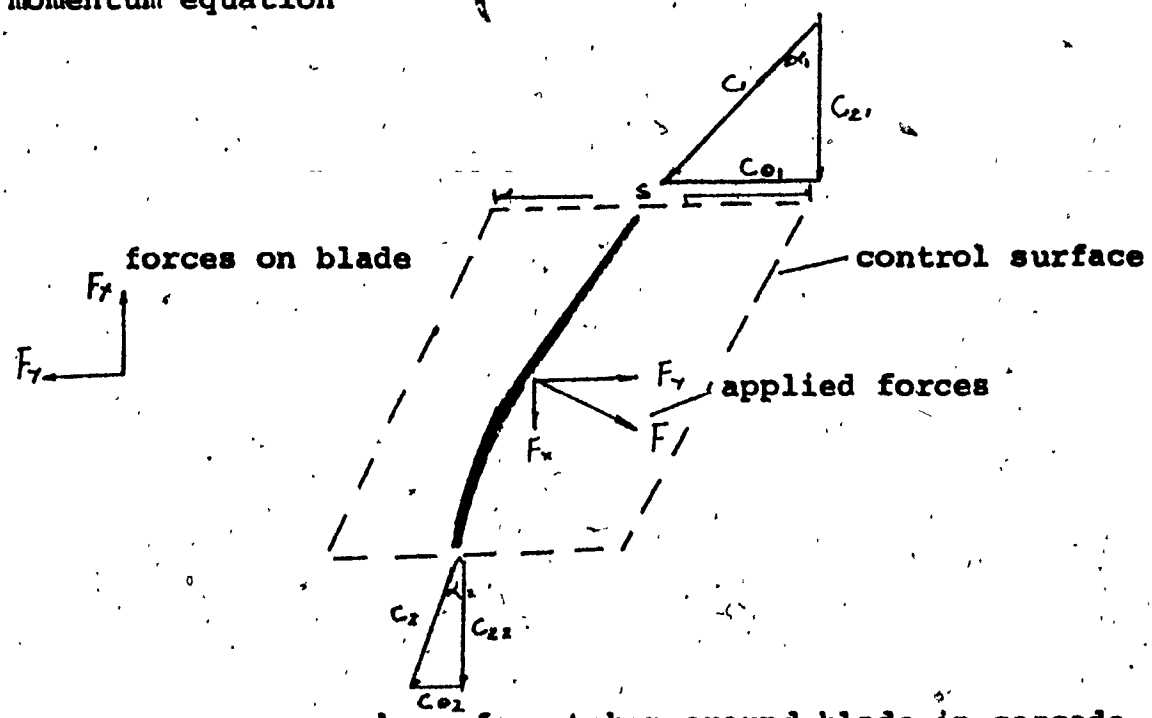

control surface taken around blade in cascade

$$F_x = (p_2 - p_1)s + (c_{x1} - c_{x2})\dot{m}$$

since $c_{x1} = c_{x2}$ (equation of continuity)

$$F_x = (p_2 - p_1)s$$

For incompressible flow the Bernoulli equation yields

$$p_1/\rho + c_1^2/2 = p_2/\rho + c_2^2/2 + \Delta p/\rho$$

where Δp = pressure losses

or $p_2 - p_1 = \frac{1}{2}\rho(c_1^2 - c_2^2) - \Delta p$

$\therefore F_x = \frac{1}{2}\rho(c_1^2 - c_2^2) - \Delta p^* s$

$= \frac{1}{2}\rho c_2^2(\tan^2\alpha_2 - \tan^2\alpha_1)s - \Delta p^* s$

Similatly, the tangential force (F_y) exerted by the fluid on eacg blade in the direction shown is given by;

$$F_y = \dot{m}(c_{\theta_1} - c_{\theta_2})$$

$$= \rho c_2 s(c_{\theta_1} - c_{\theta_2}) \qquad (\dot{m} = \rho c_2 s)$$

$$= \rho c_2^2 s(\tan\alpha_2 - \tan\alpha_1)$$

The mean velocity through the cascade is

$$c_m = c_2 \sec\alpha_m$$

where $\tan\alpha_m = (\tan\alpha_1 + \tan\alpha_2)/2$

Thus, the lift force (F_L) perpendicular to the mean velocity (c_m) is

$$F_L = F_x \sin\alpha_m + F_y \cos\alpha_m$$

$$= \frac{1}{2}\rho c_2^2 s(\tan^2\alpha_1 - \tan^2\alpha_2)\sin\alpha_m$$

$$= \rho c_2^2 s^* \sec\alpha_m(\tan\alpha_1 - \tan\alpha_2) - \Delta p^* s^* \sin\alpha_m$$

And the lift coefficient is defined as

$$C_L = F_L/(\frac{1}{2}\rho c_m^2 l)$$

$$= 2(s/l)(\tan\alpha_1 - \tan\alpha_2)\cos\alpha_m - \Delta p(s/l)\sin\alpha_m/(\frac{1}{2}\rho c_m^2)$$

The lift coefficient represents the aerodynamic loading of a blade.

The drag force (F_D) parallel to the mean velocity (c_m) is

$$F_D = F_y \sin\alpha_m + F_x \cos\alpha_m$$

$$= \Delta p s^* \cos\alpha_m$$

and $$C_D = F_D / (\tfrac{1}{2}\rho c_1^2 l)$$

$$= \Delta p / (\tfrac{1}{2}\rho c_1^2)(s/l)\cos^2\alpha_2/\cos^2\alpha_1$$

The loss coefficient ($\bar{\omega}$) is defined as

$$\bar{\omega} = \Delta p / (\tfrac{1}{2}\rho c_1^2)$$

Hence, $C_D = \bar{\omega}(s/l)\cos^2\alpha_2/\cos^2\alpha_1$.

For a particular cascade, s/l, α_1 and α_m are constants, we have the results that the drag coefficient is directly proportional to the loss coefficient ($\bar{\omega}$).

$$C_D \propto \bar{\omega} \quad \text{----------(5.1)}$$

The lift coefficient may now be rewritten

$$C_L = 2(s/l)(\tan\alpha_1 - \tan\alpha_2)\cos\alpha_2 - C_D \tan\alpha_m$$

This means C_L will increase while C_D decreases.

The relationship between the above coefficients and the Reynolds number can be established from the theorectical integrated drag coefficient for imcompressible flow on a flat plate. The results of Von-Karman and Prandtl on C_D vs R_c based on turbulent formulation are shown as below:

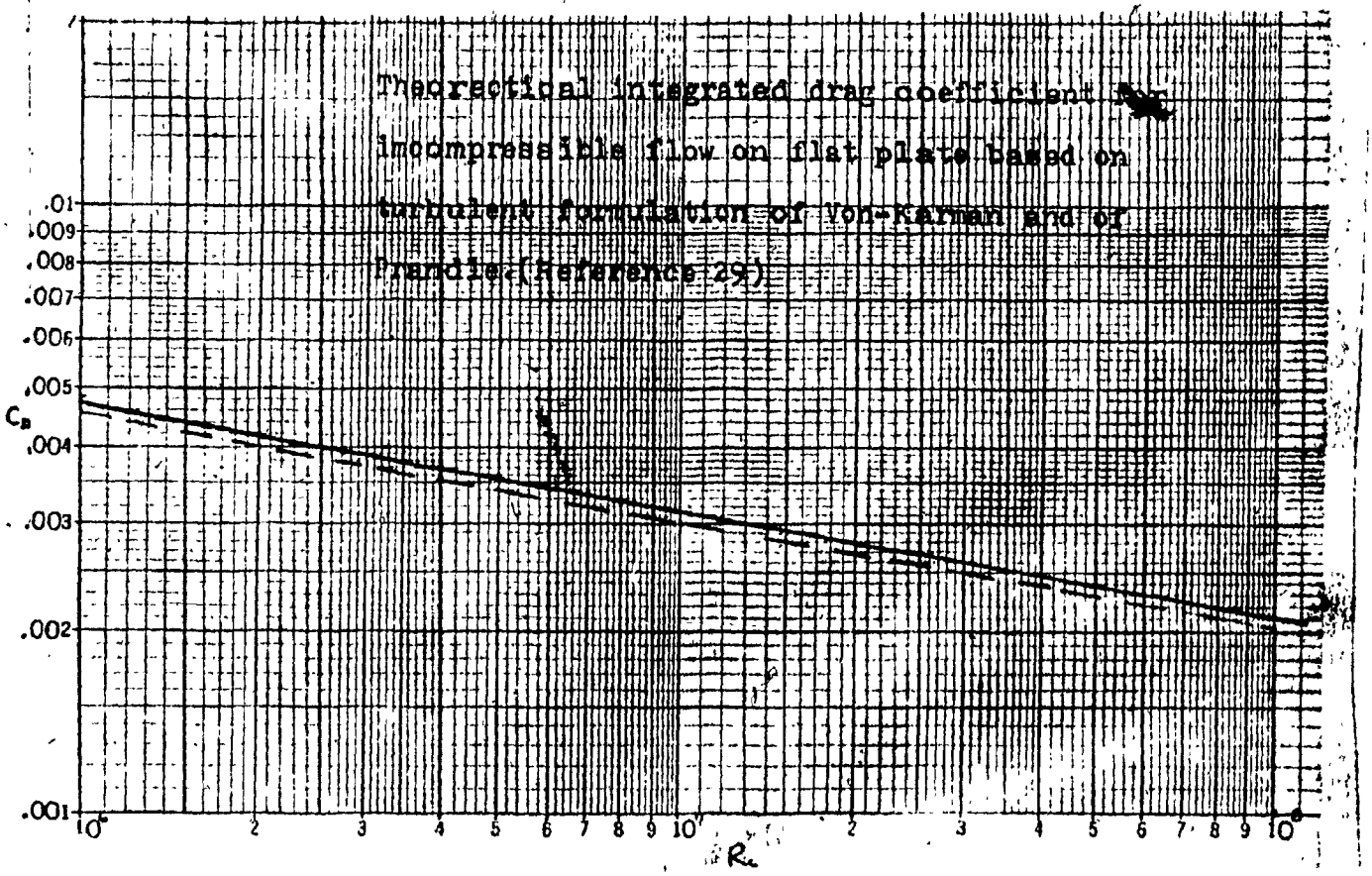

Note that the relation between C_D and C_f is given by reference 29 as

$$C_D = \frac{\int_0^x \tau_w \, dx}{\frac{1}{2}\rho V^2 x} = \frac{1}{x}\int_0^x \frac{\tau_w \, dx}{\frac{1}{2}\rho V^2} = \frac{1}{x}\int_0^x C_f \, dx$$

It follows that

$$C_f = \frac{d[C_D x]}{dx} = C_D + x\frac{dC_D}{dx}$$

$$= C_D + R_x \frac{dC_D}{dR_x}$$

$$= C_D\left[1 + \frac{d[\ln C_D]}{d[\ln R_x]}\right]$$

Hence, given a curve of Ln C_D vs Ln R_c, the variation of local skin-friction coefficient with Reynolds number may be found by differentiation as indicated by the above equation. Graphically, the term $d(\text{Ln } C_D)/d(\text{Ln } R_c)$ can be evaluated from the slope of the curve of Ln C_D vs Ln R_c. The avaerage slope in the above graph is about (-.176), therefore the value of C_f is approximately equal to .424 of the value of C_D.

From the above analysis, we can conclude that

$$C_f = .424\, C_D$$

or

$$C_f \propto C_D$$

and

$$C_D \propto R_c^{-.176} \qquad \text{----------(5.2)}$$

finally,

$$C_f \propto R_c^{-.176} \qquad \text{----------(5.3)}$$

$$\bar{\omega} \propto C_D \propto R_c^{-.176} \qquad \text{----------(5.4)}$$

These results (equation 5.1, 5.2, 5.3 and 5.4) are in close agreement with equation (2), Chapter 2.0. and equation (48), Chapter 9.0.

APPENDIX

Illustration of Graphs and Figures

Figure 1 Diagramatic Sketch of compressor Map
Showing Effect of Reynolds Number
On compressor Performance

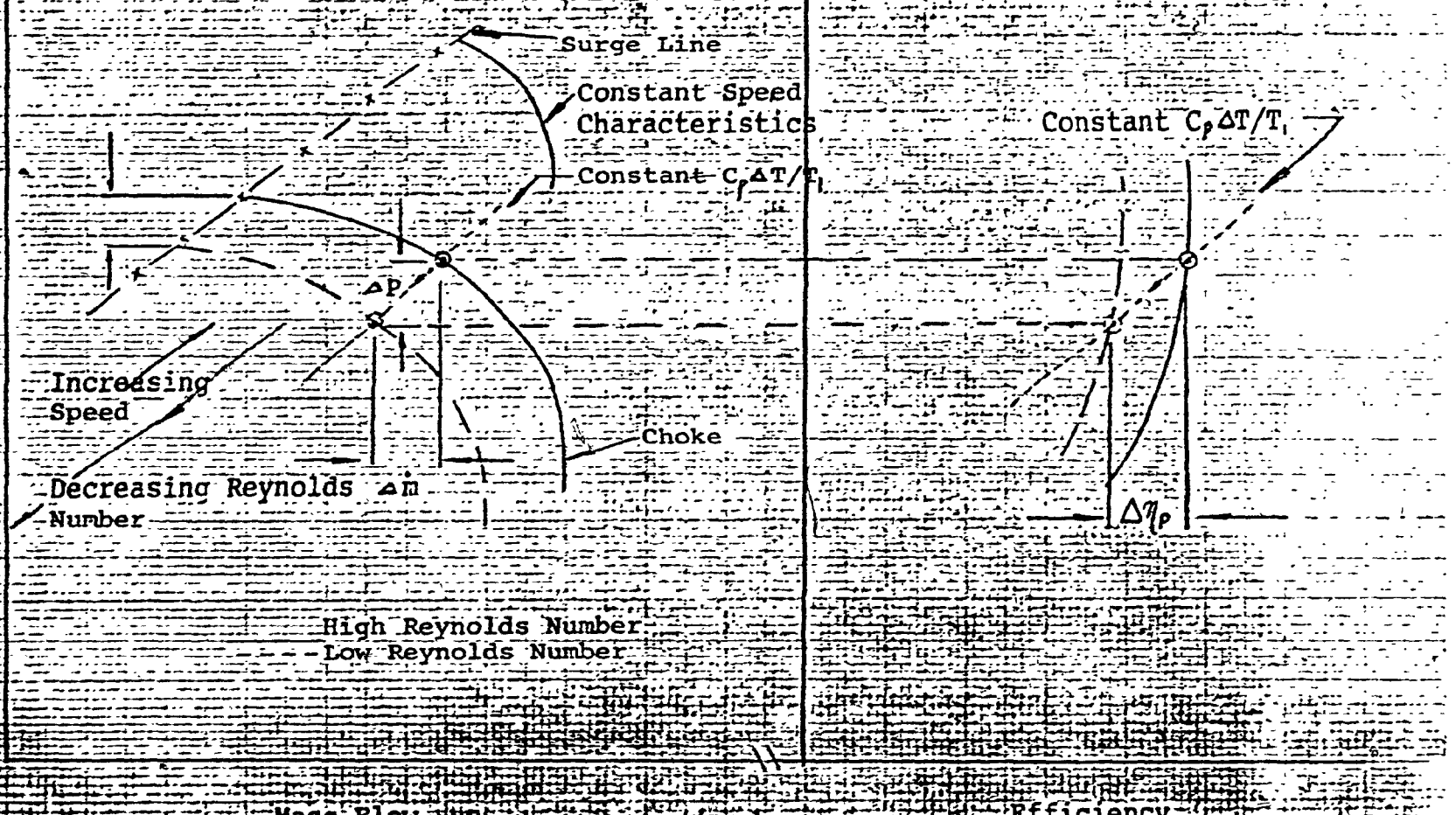

Figure 2 Variation of Maximum Efficiency And Peak Pressure Coefficient With Reynolds Number. (Ref.8)

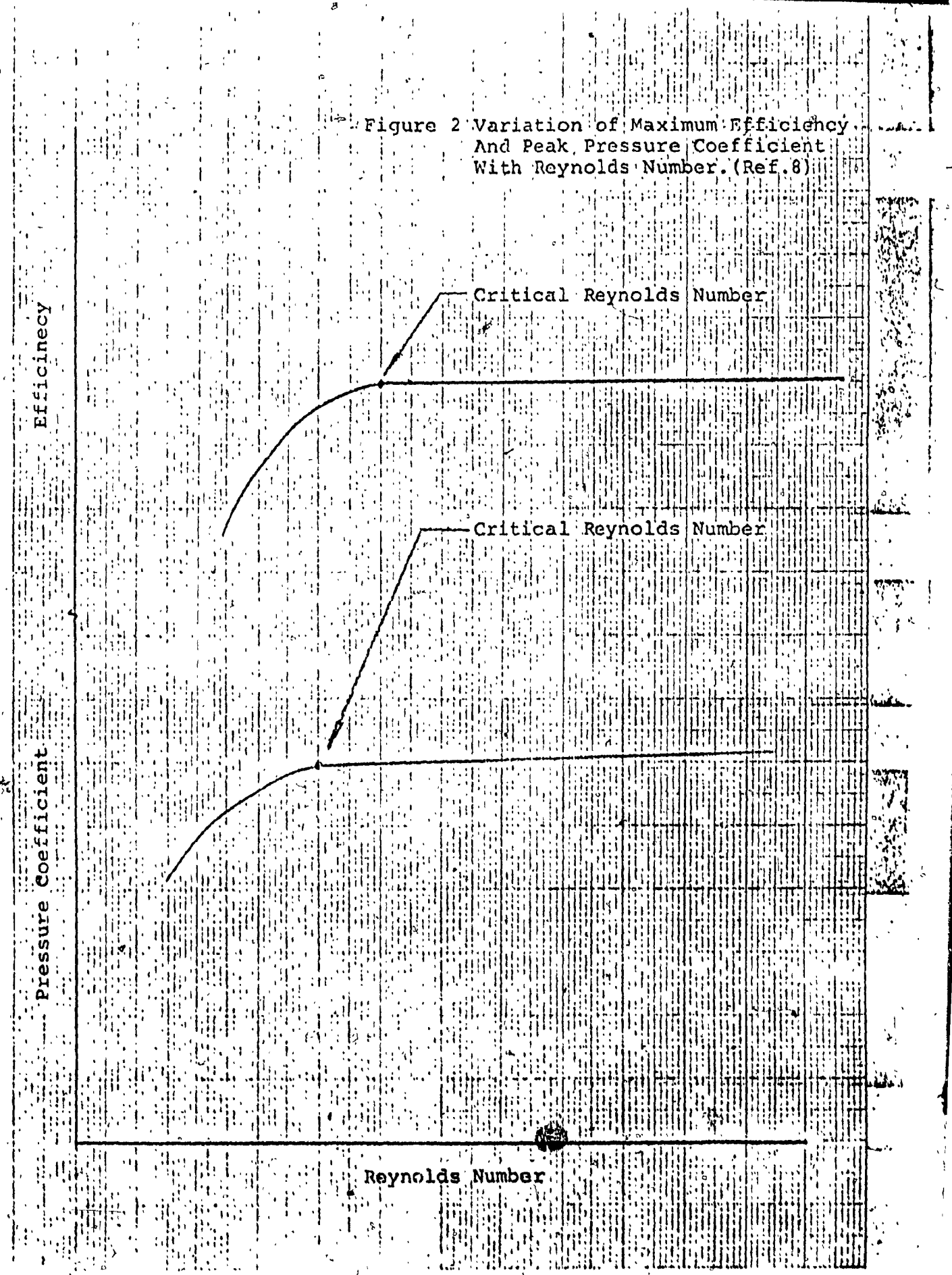

Figure 3. Drag and Drag Coefficient of Sphere
In Region of Critical Reynolds Number

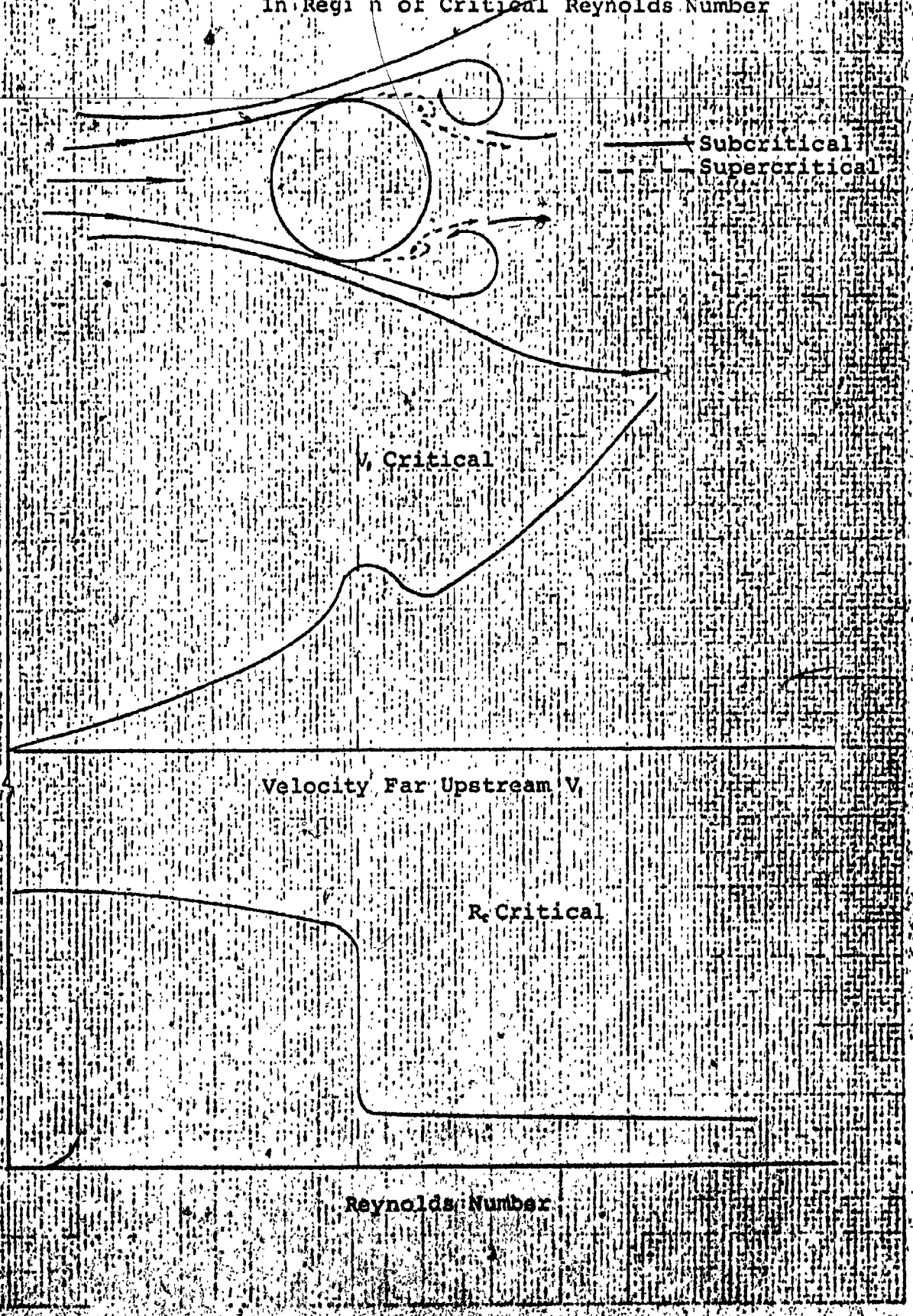

Figure 4. Potential-theorectical Velocity Distribution Showing Calculated Point of Laminar Separation for The Joukowski Profile (Reference 5)

For definition of C_1 see Appendix V

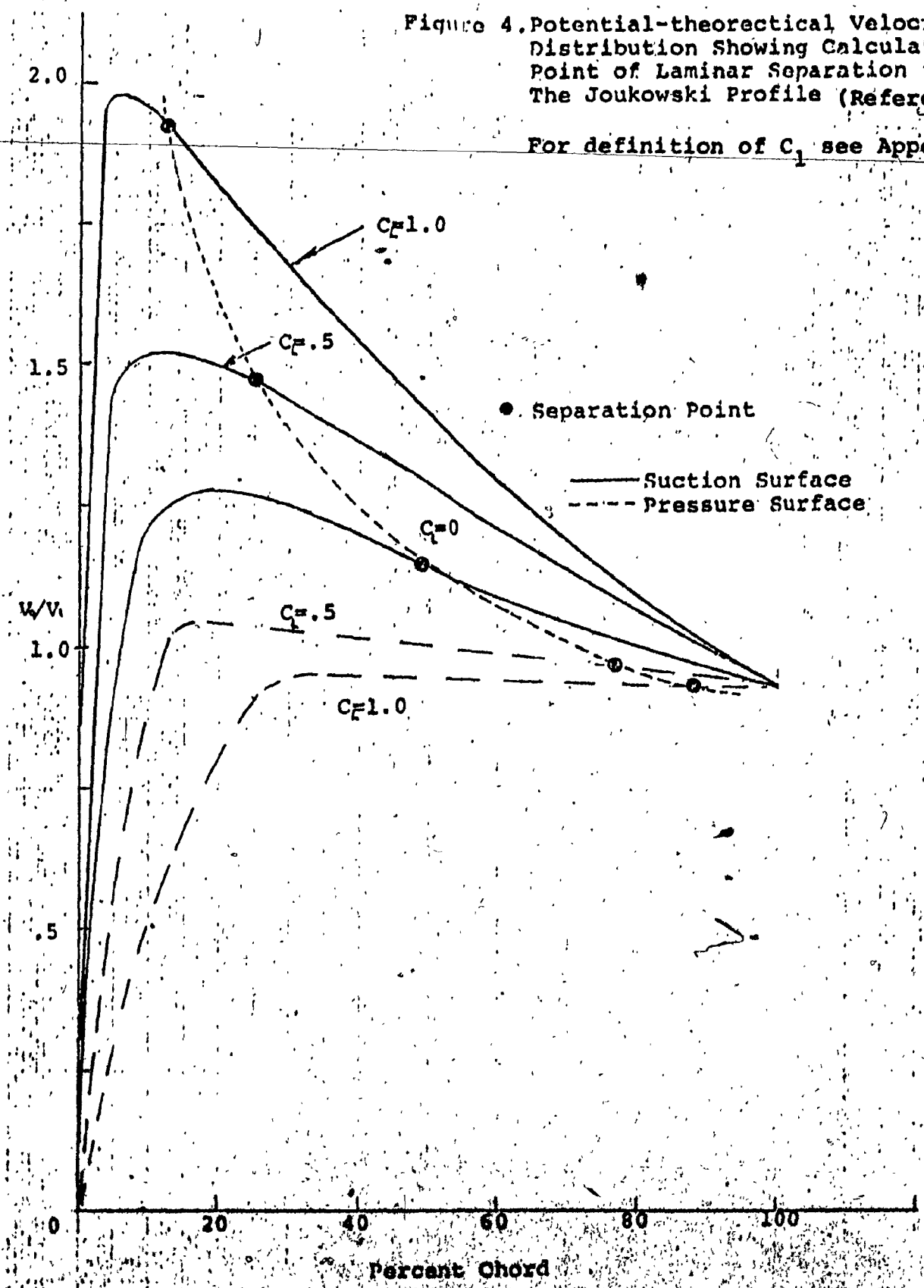

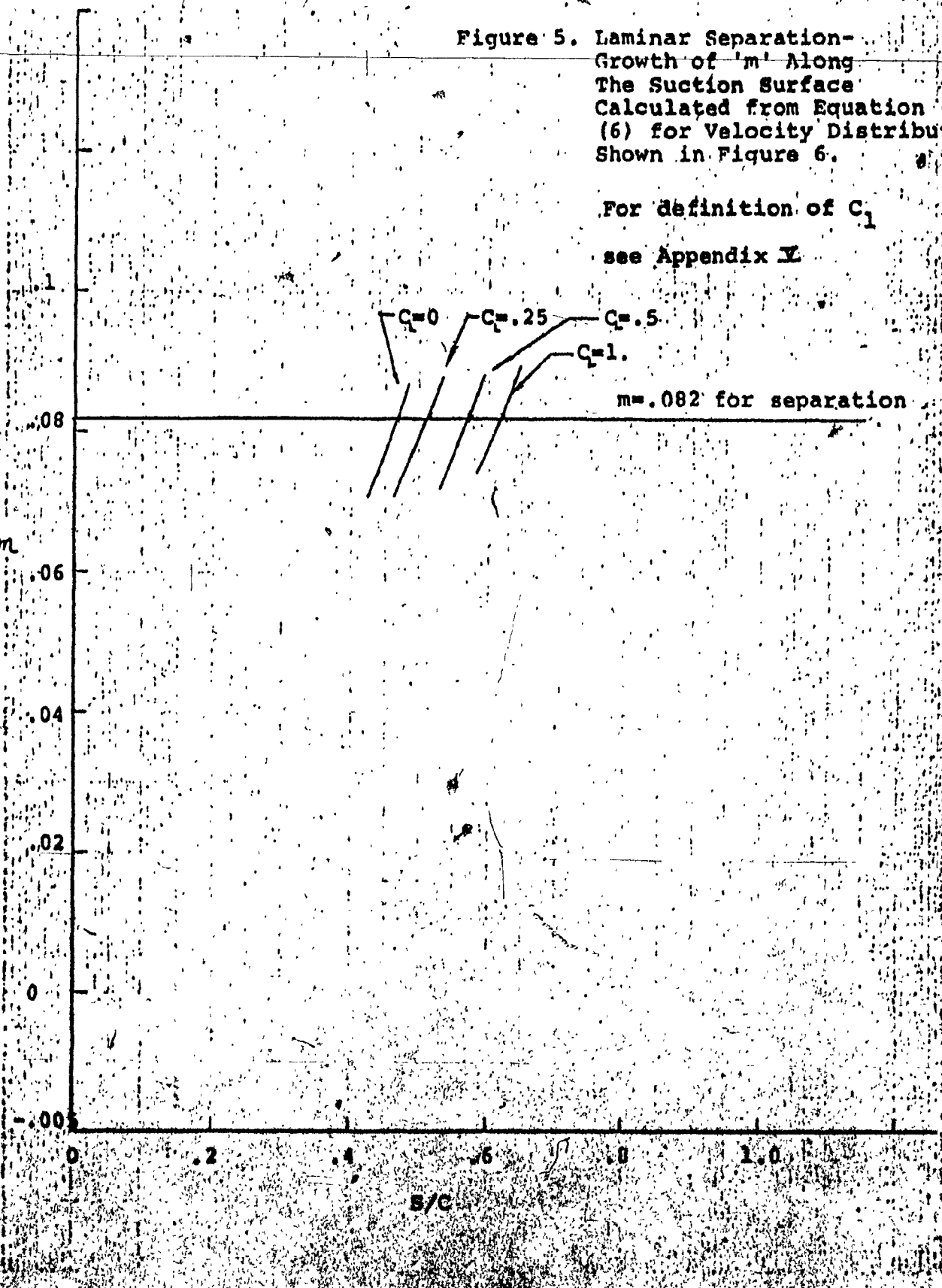

Figure 5. Laminar Separation- Growth of 'm' Along The Suction Surface Calculated from Equation (6) for Velocity Distribution Shown in Figure 6.

For definition of C_l see Appendix X

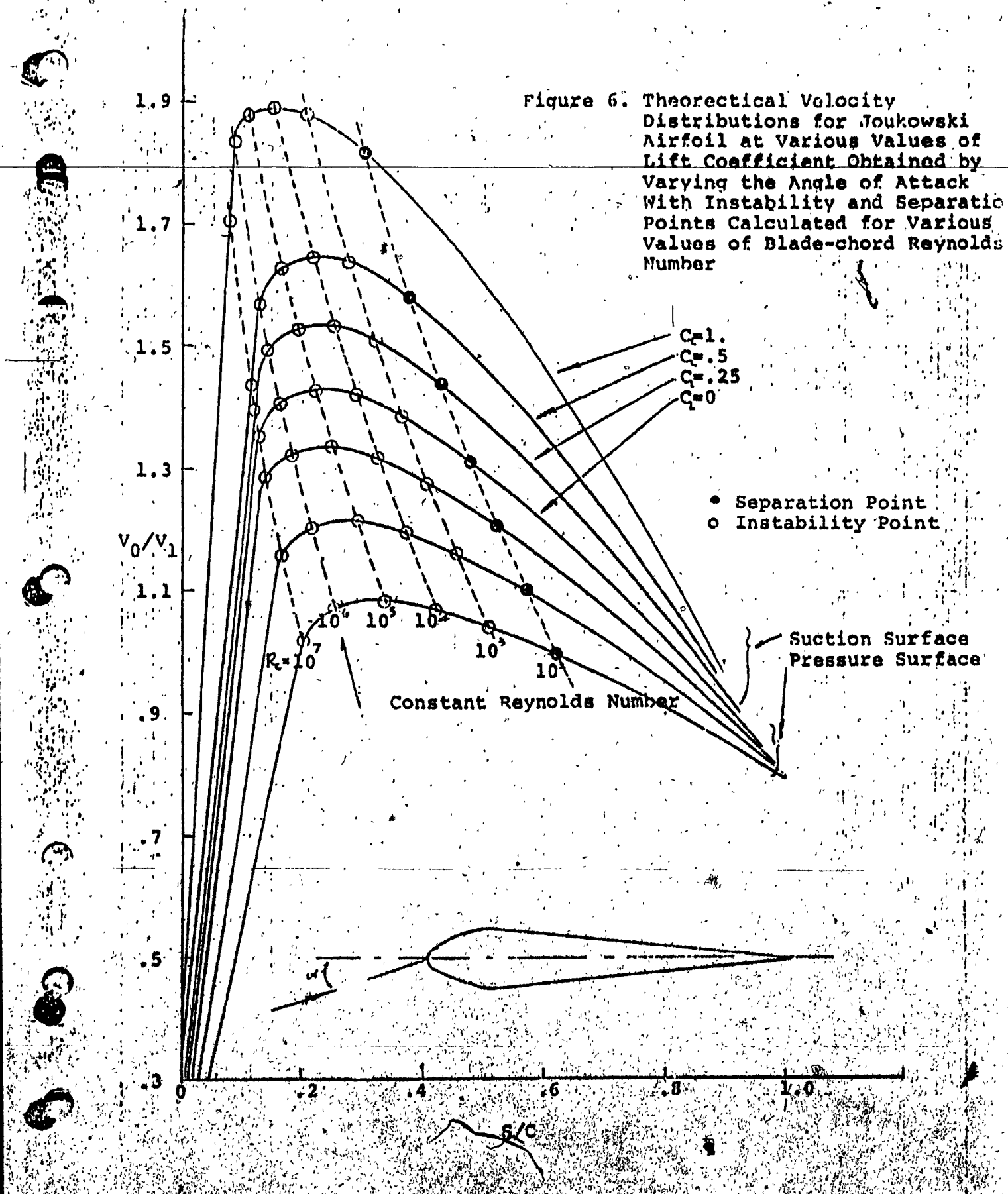

Figure 6. Theorectical Velocity Distributions for Joukowski Airfoil at Various Values of Lift Coefficient Obtained by Varying the Angle of Attack With Instability and Separatio Points Calculated for Various Values of Blade-chord Reynolds Number

Figure 7. Typical Onset of Transition Boundary Layer Calculated from a Set of Modeling Equations (ref.13)

Note λ =Scale Length

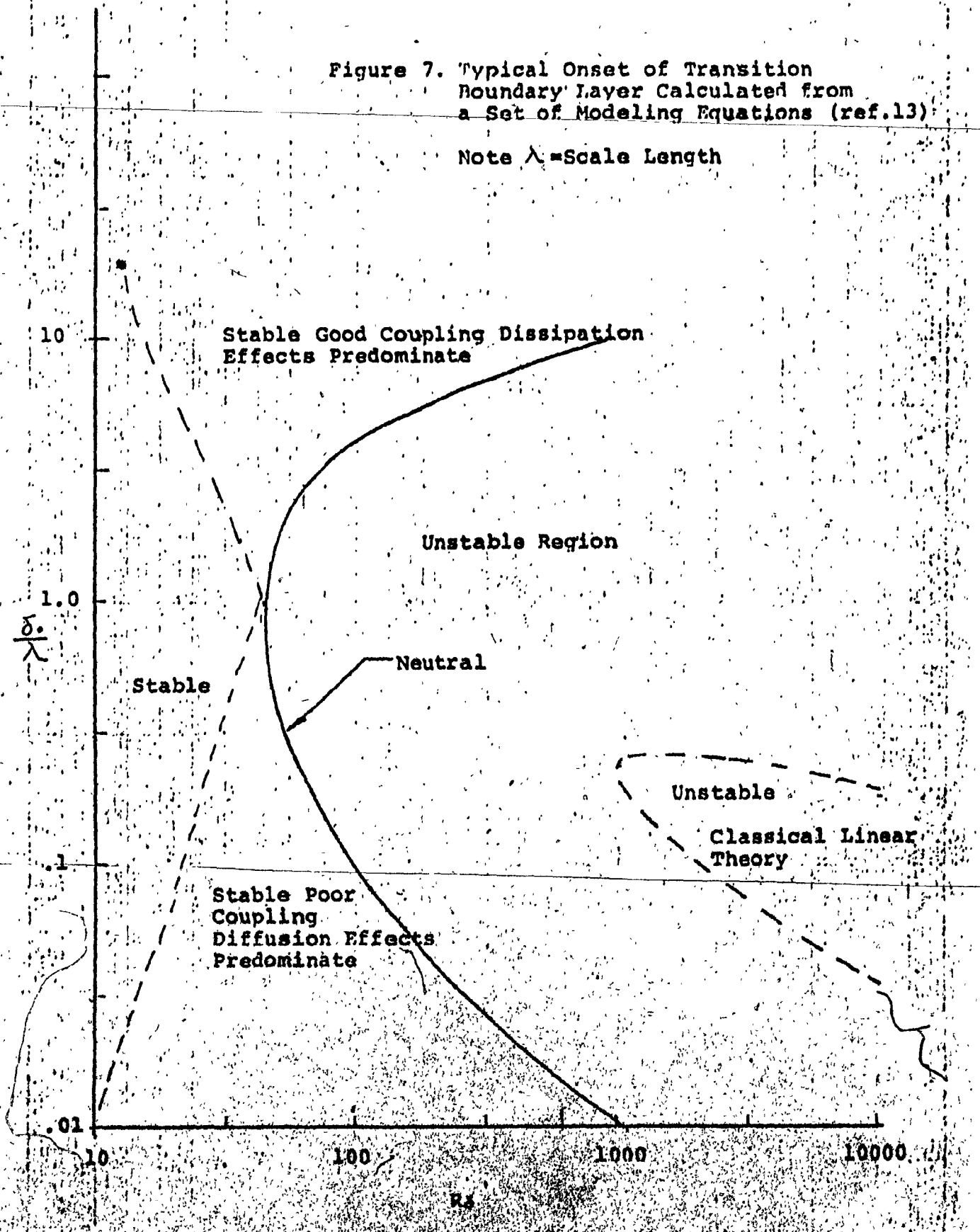

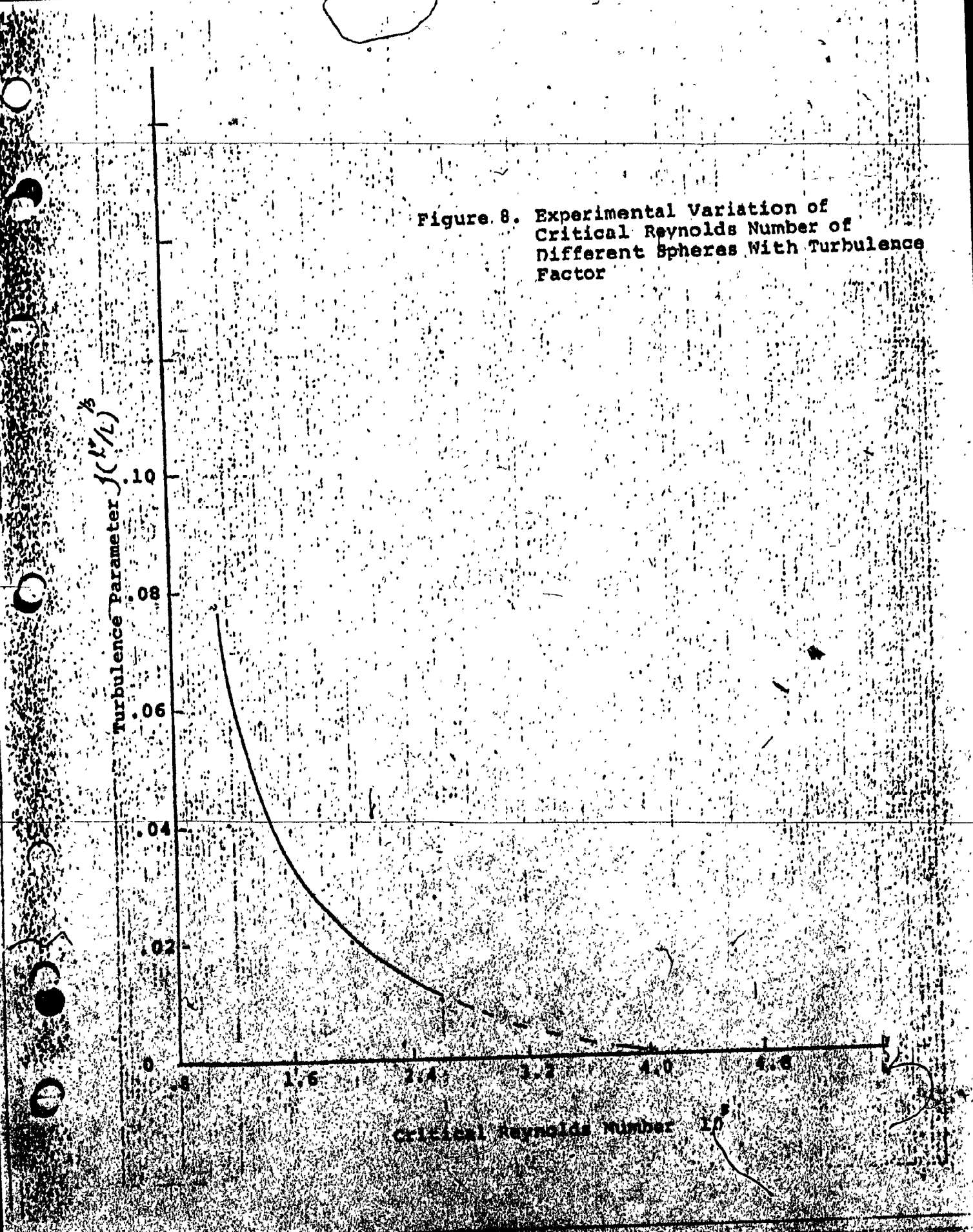

Figure 8. Experimental Variation of Critical Reynolds Number of Different Spheres With Turbulence Factor

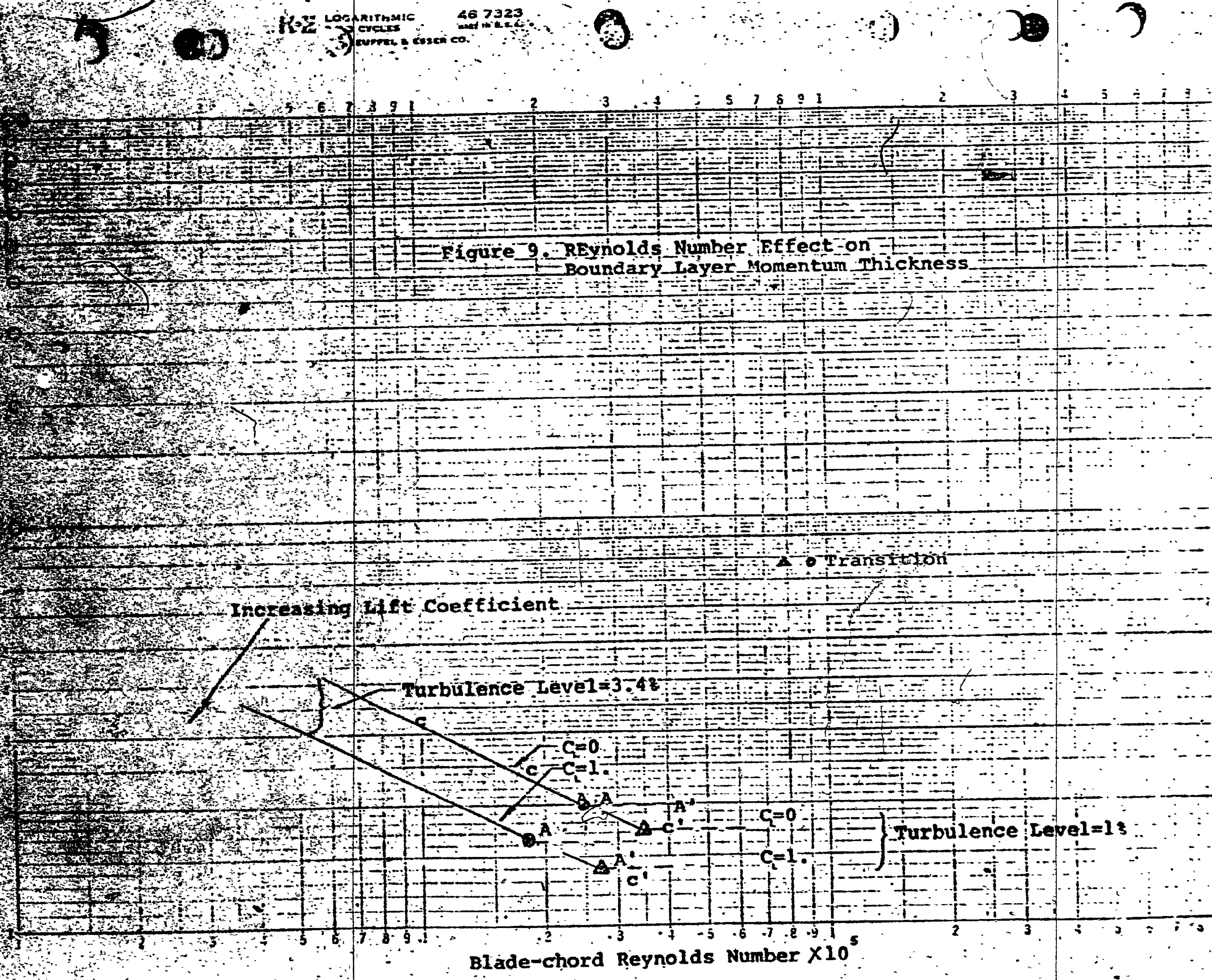

Figure 9. REynolds Number Effect on Boundary Layer Momentum Thickness

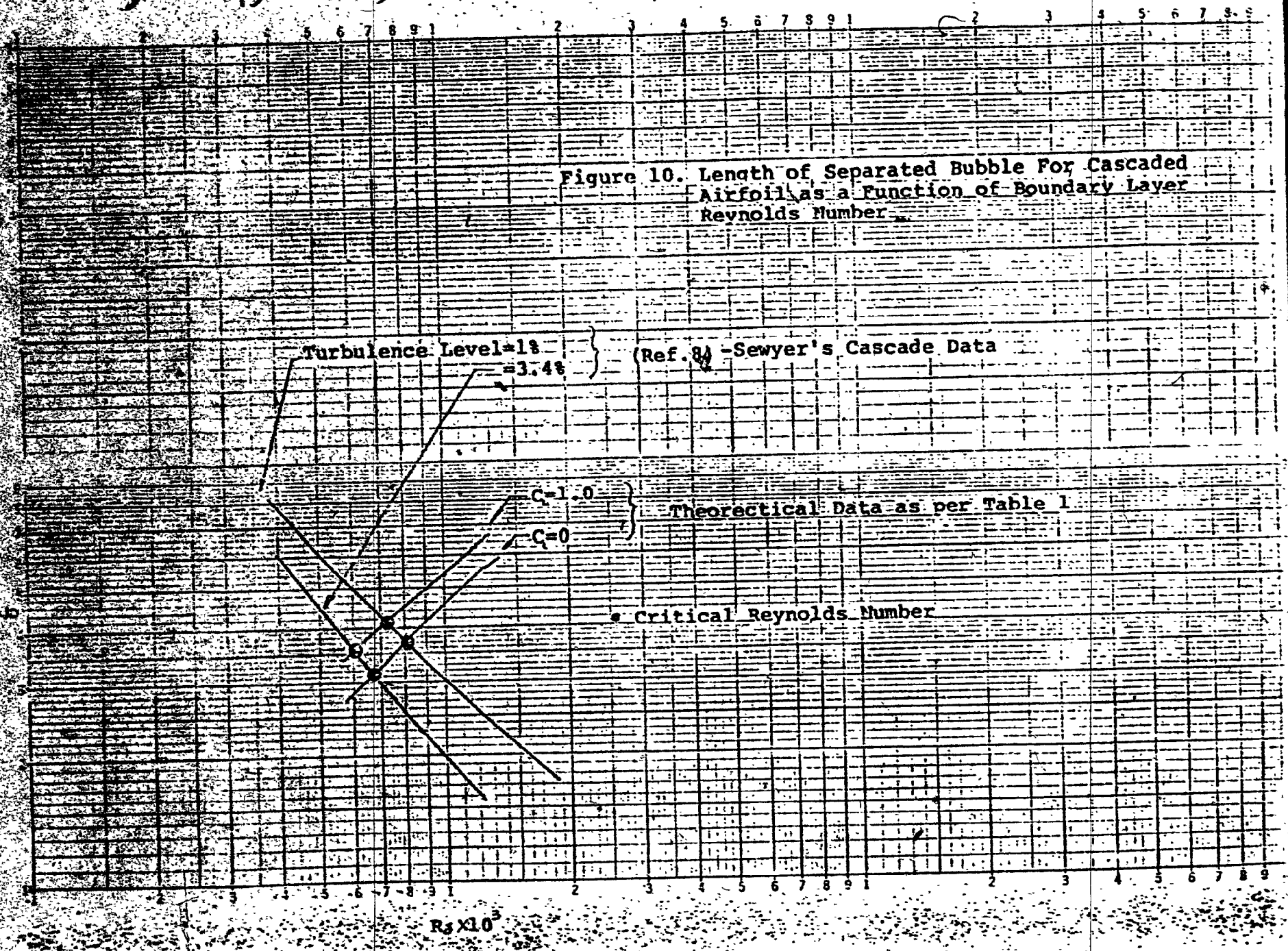

Figure 10. Length of Separated Bubble For Cascaded Airfoil as a Function of Boundary Layer Reynolds Number

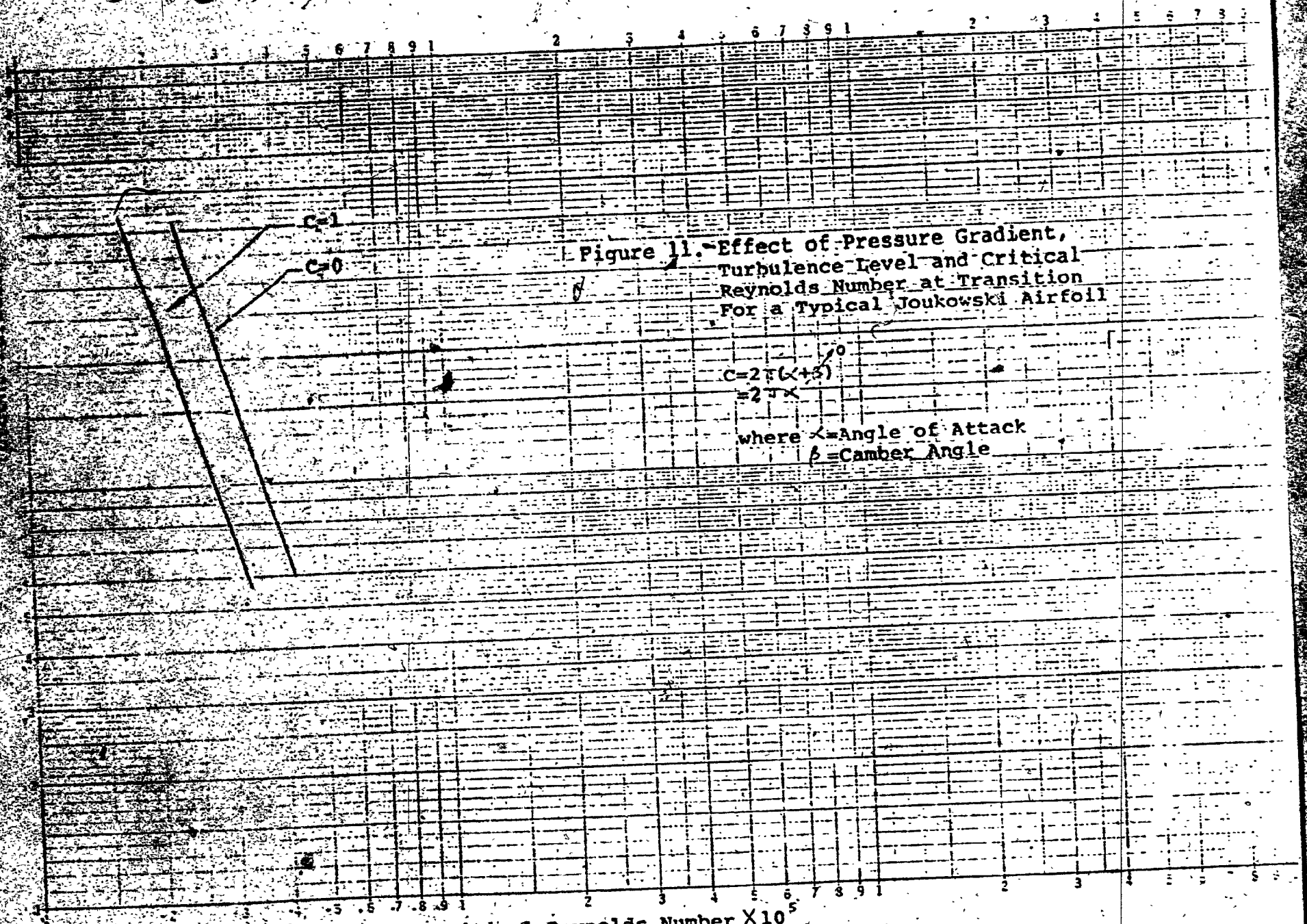

Figure 11. Effect of Pressure Gradient, Turbulence Level and Critical Reynolds Number at Transition For a Typical Joukowski Airfoil

$$C = 2\pi(\alpha+\beta)^0$$
$$= 2\pi\alpha$$

where α=Angle of Attack
β=Camber Angle

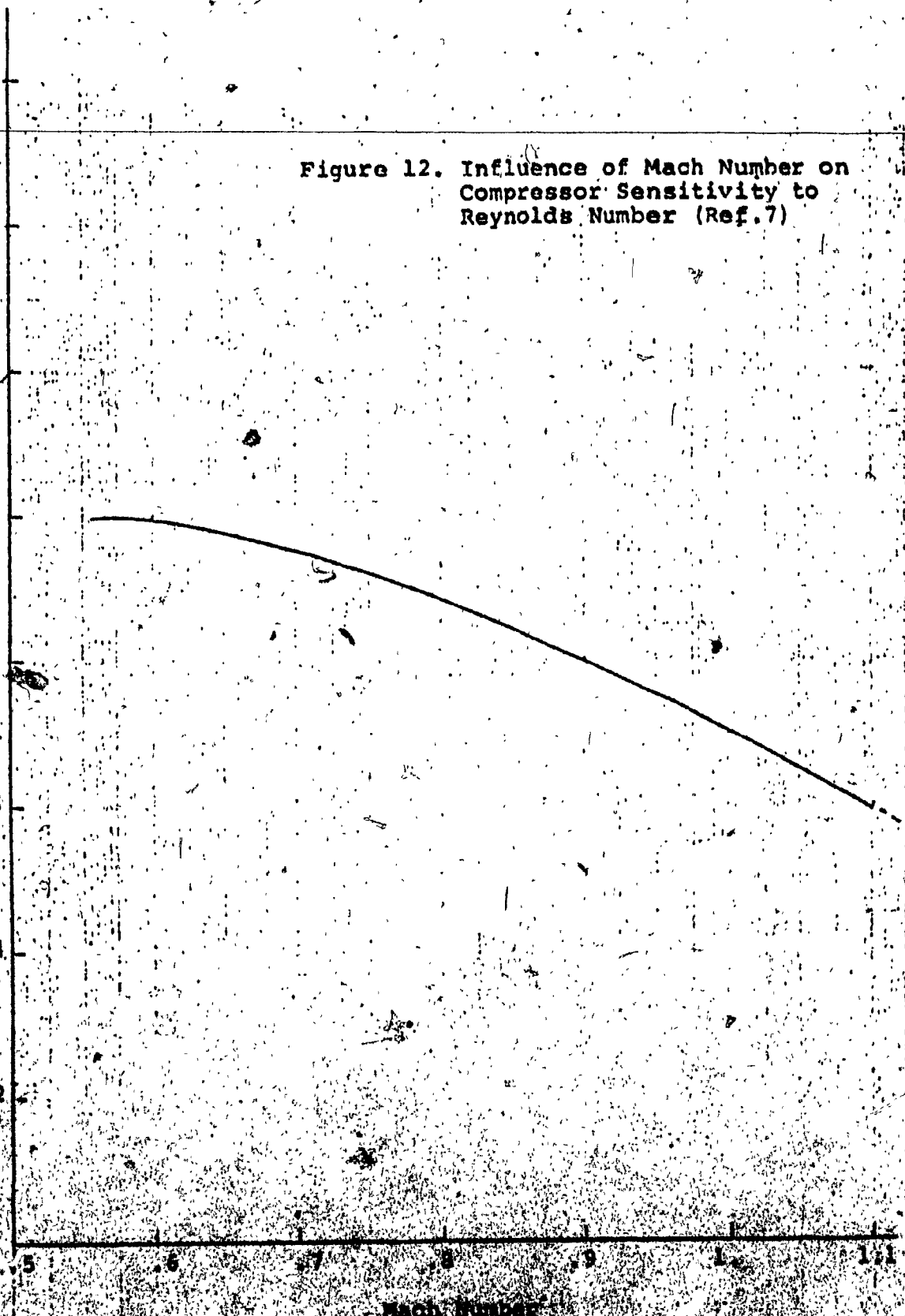

Figure 12. Influence of Mach Number on Compressor Sensitivity to Reynolds Number (Ref.7)

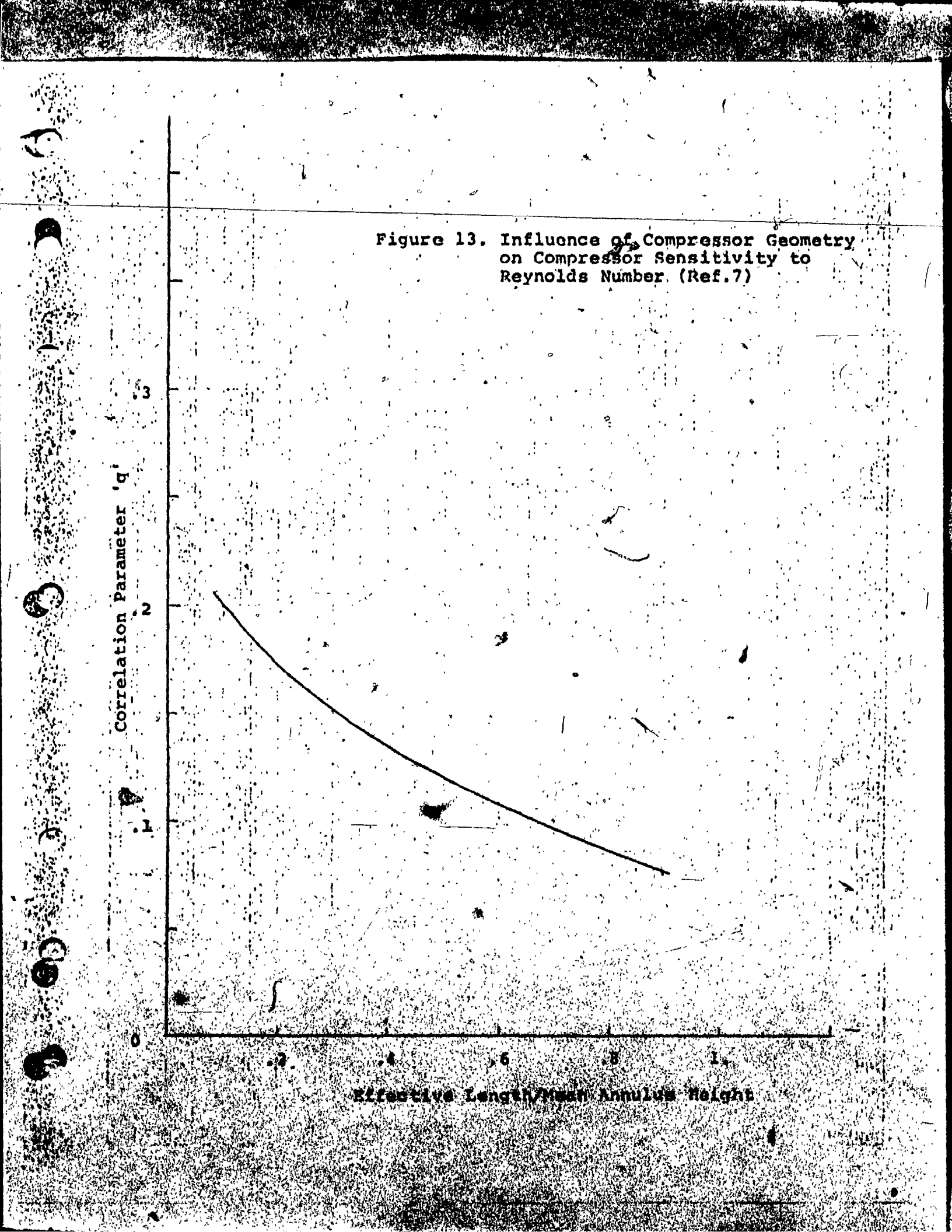

Figure 13. Influence of Compressor Geometry on Compressor Sensitivity to Reynolds Number. (Ref.7)

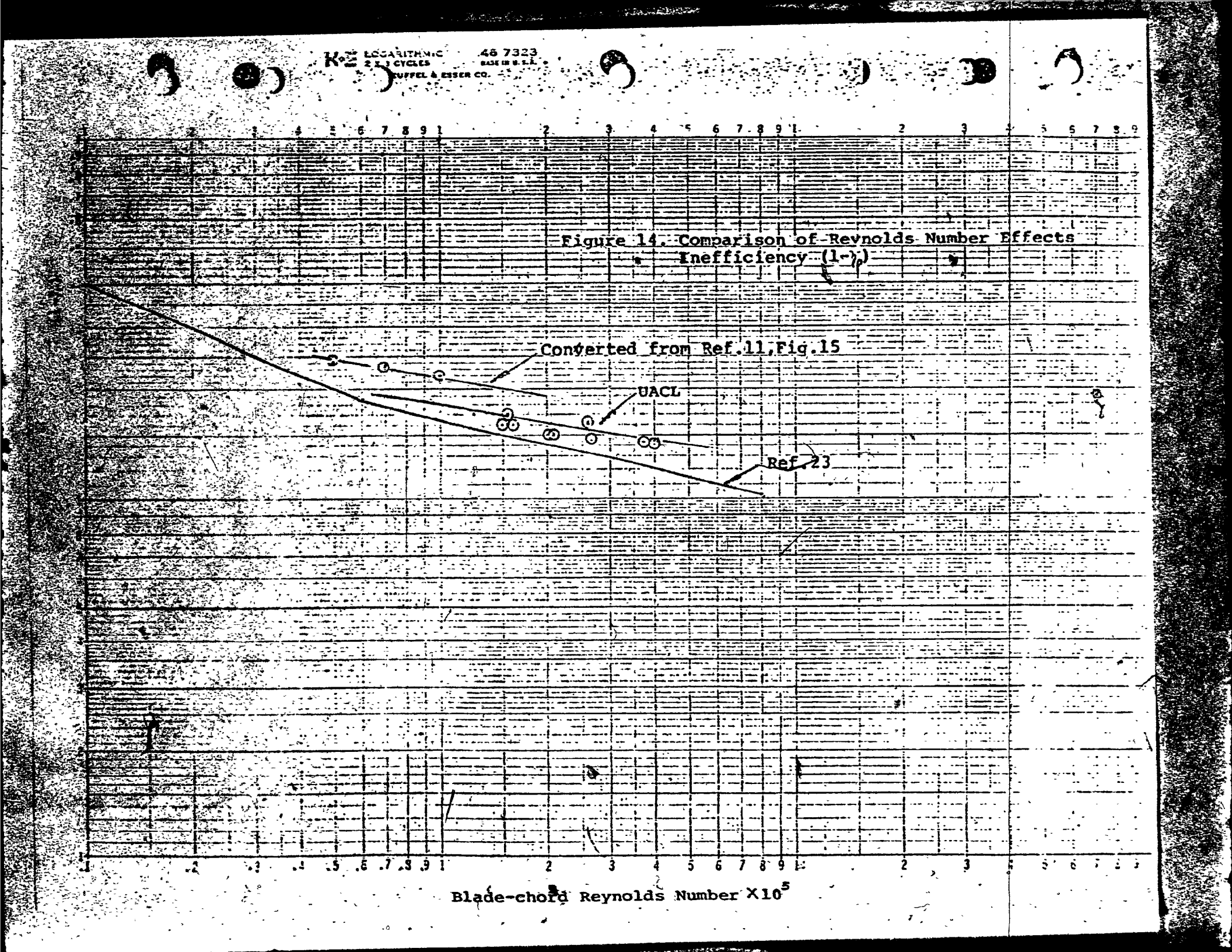

Figure 14. Comparison of Reynolds Number Effects
Inefficiency $(1-\eta_p)$

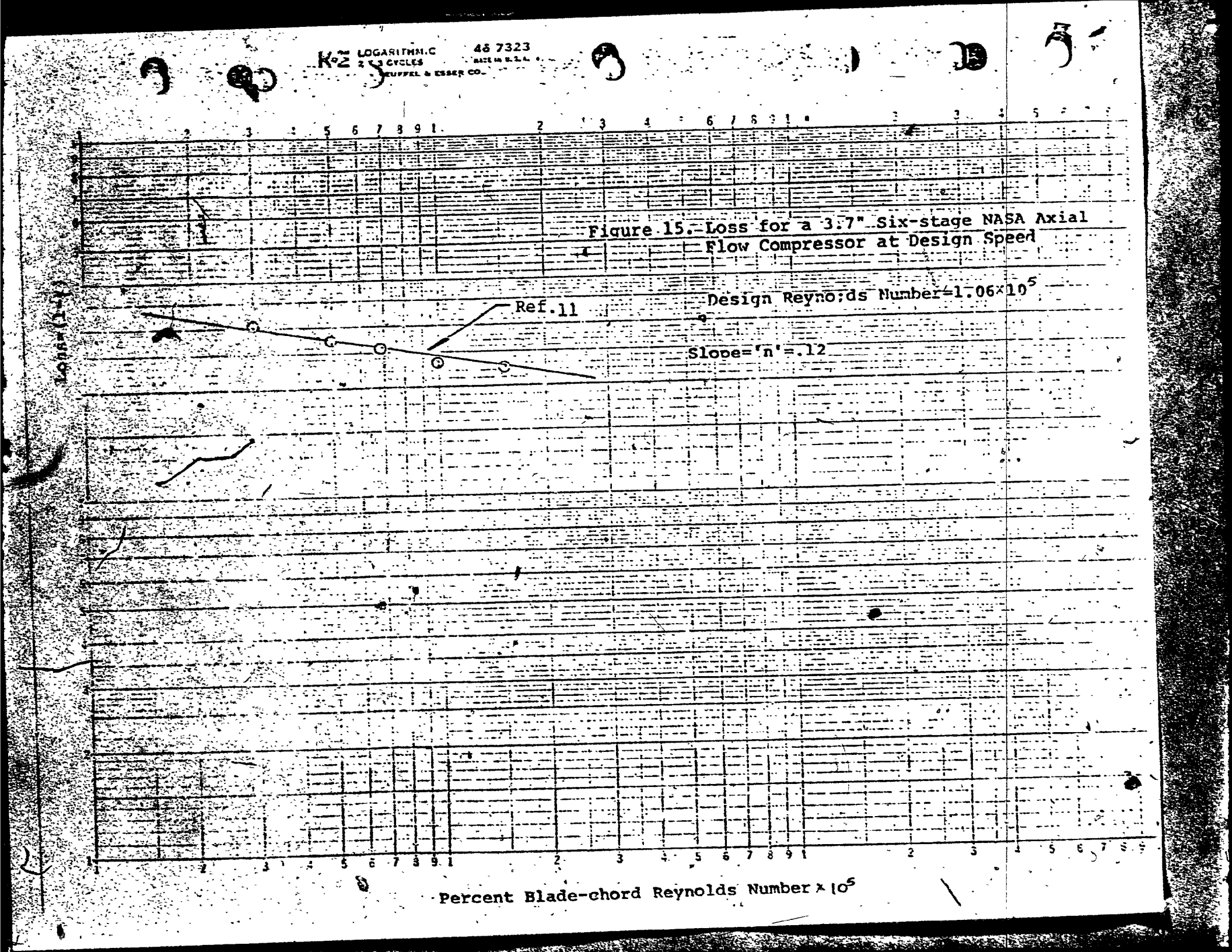

Figure 15.- Loss for a 3.7" Six-stage NASA Axial Flow Compressor at Design Speed

Figure 16. Compressor Work Factor as a Function of Percent Design Equivalent Weight Flow for Various Reynolds Numbers (Ref. 12)

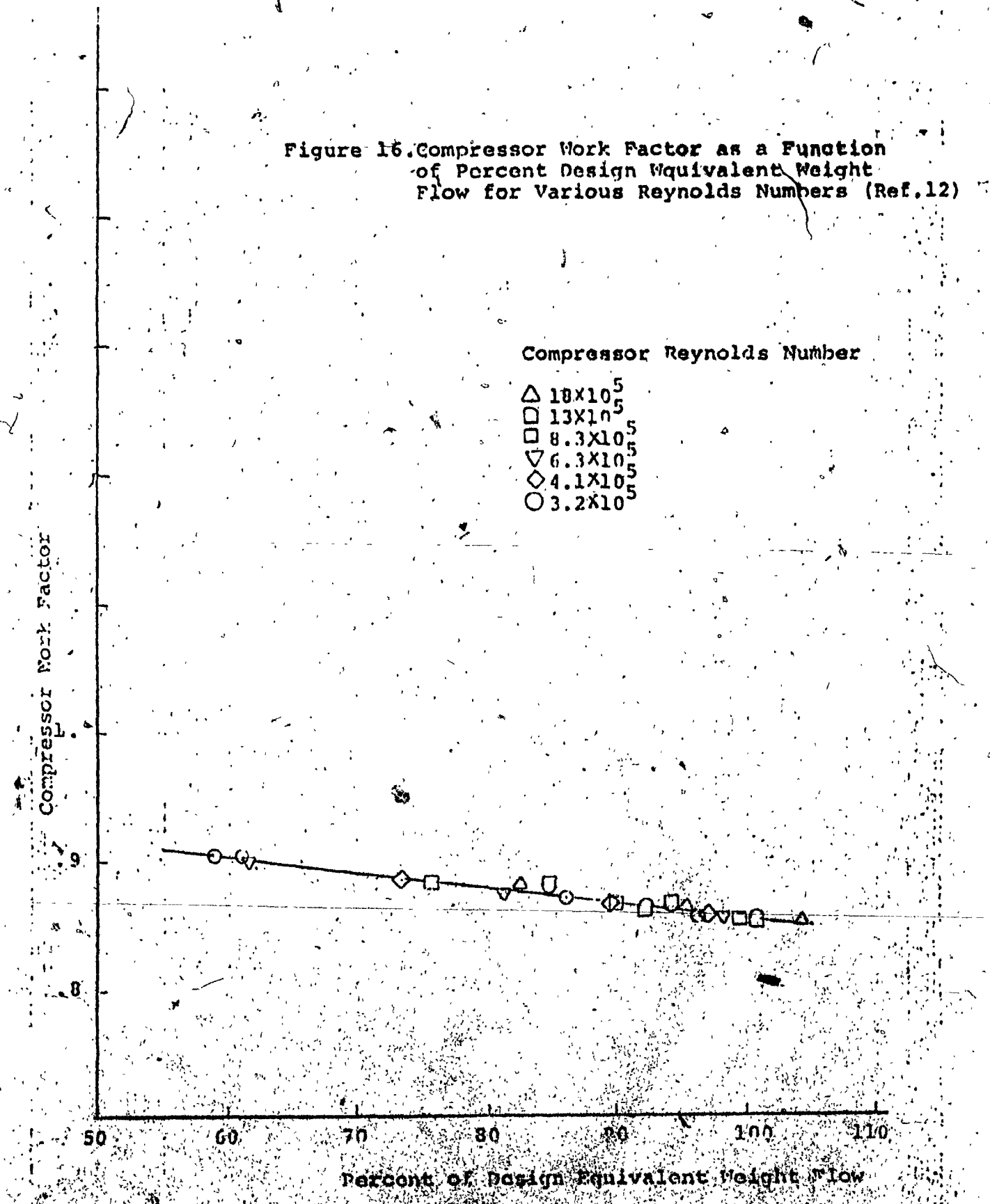

Figure 17. Comparison of Overall Pressure Ratio and Flow Range at Various Reynolds Numbers for a 6" Centrifugal Compressor at Design Speed (Ref. 12)

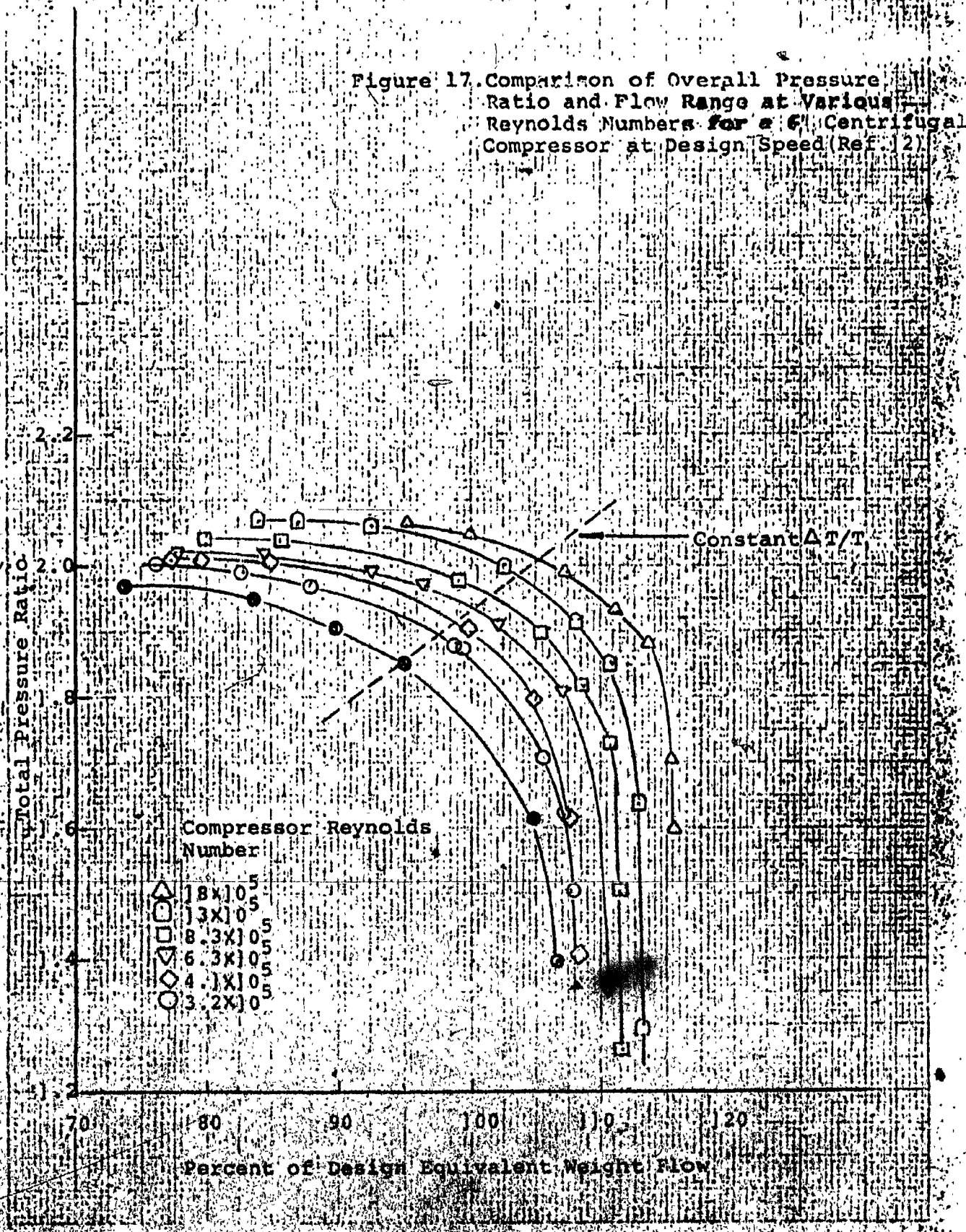

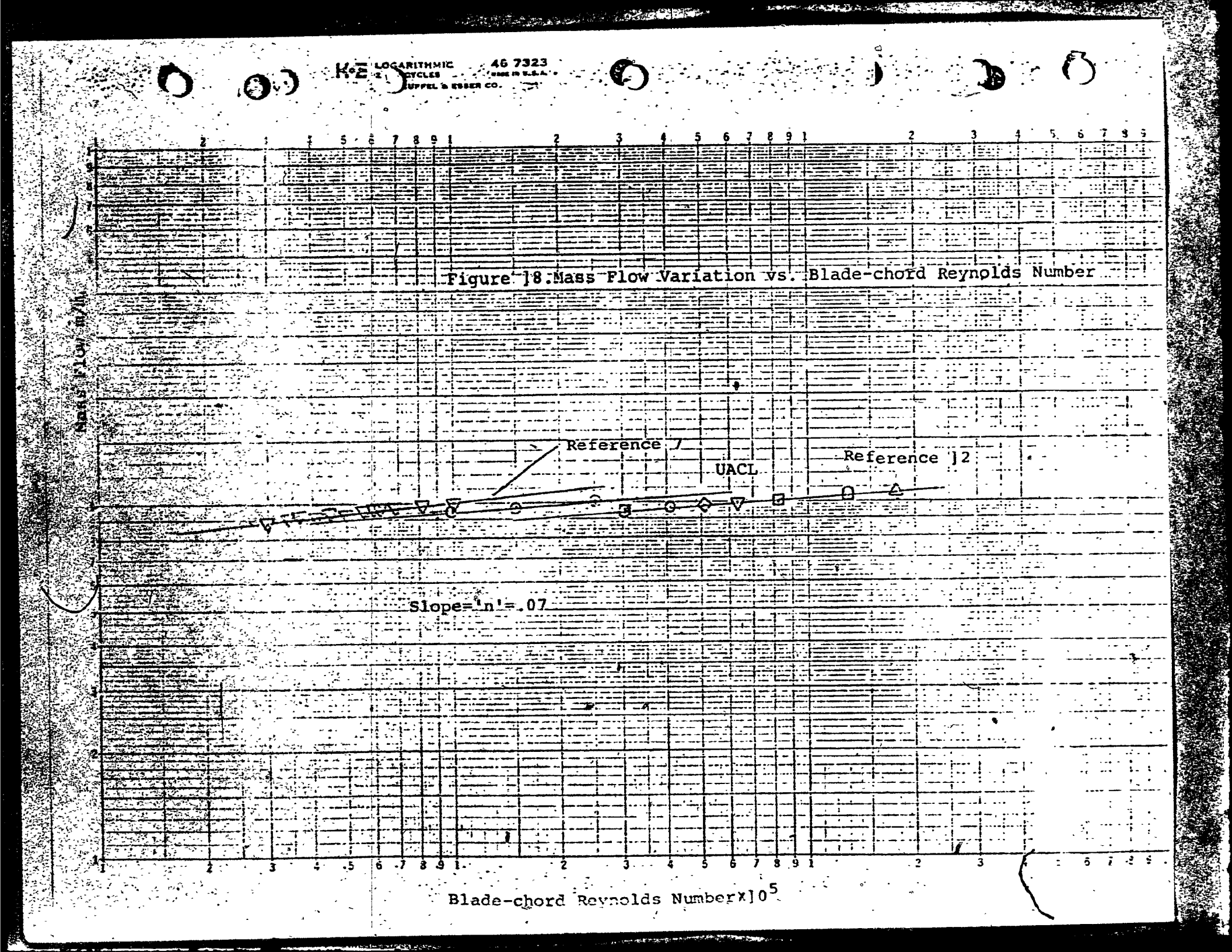

Figure 18. Mass Flow Variation vs. Blade-chord Reynolds Number

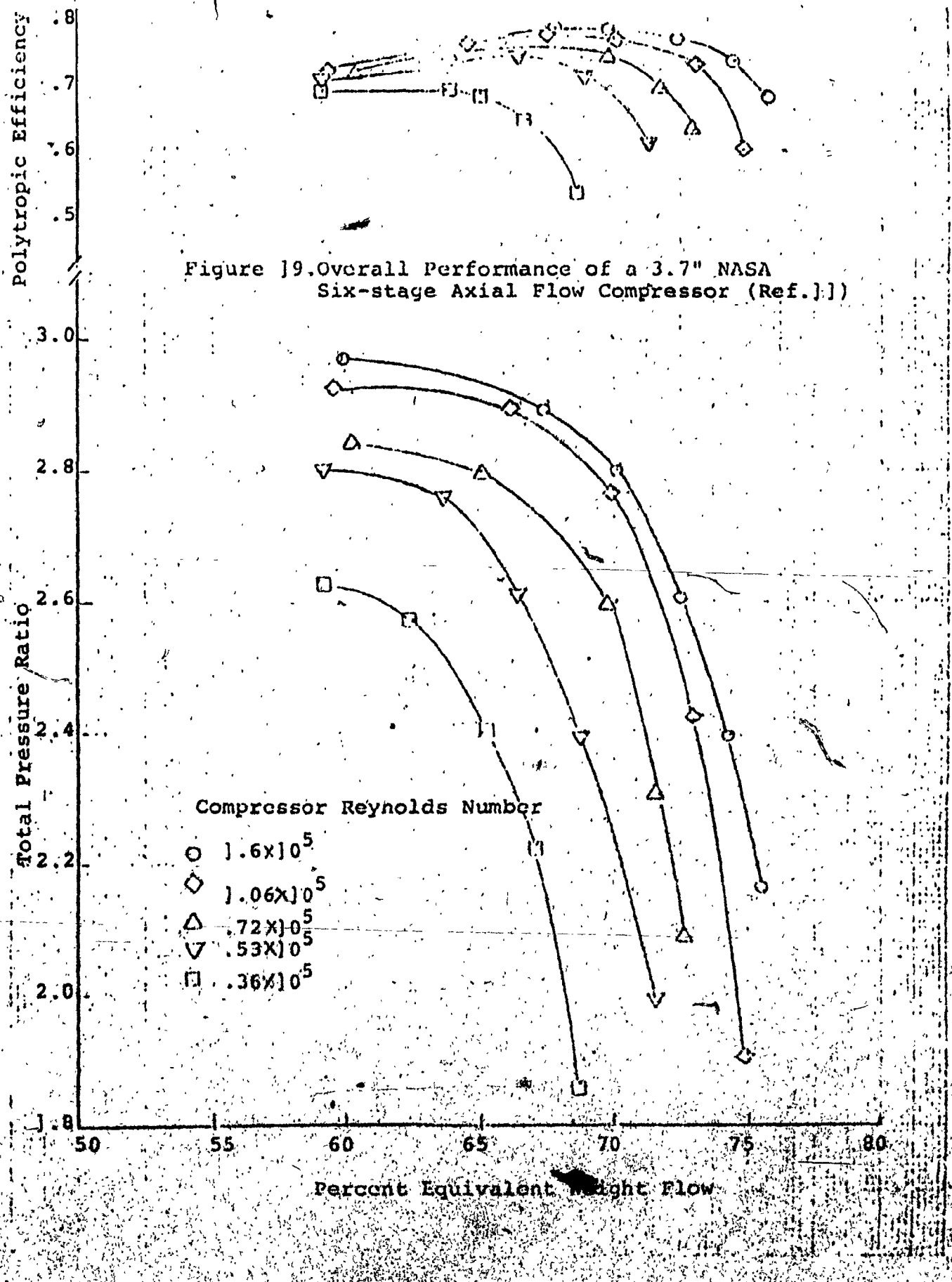

Figure 19. Overall Performance of a 3.7" NASA Six-stage Axial Flow Compressor (Ref. 1)

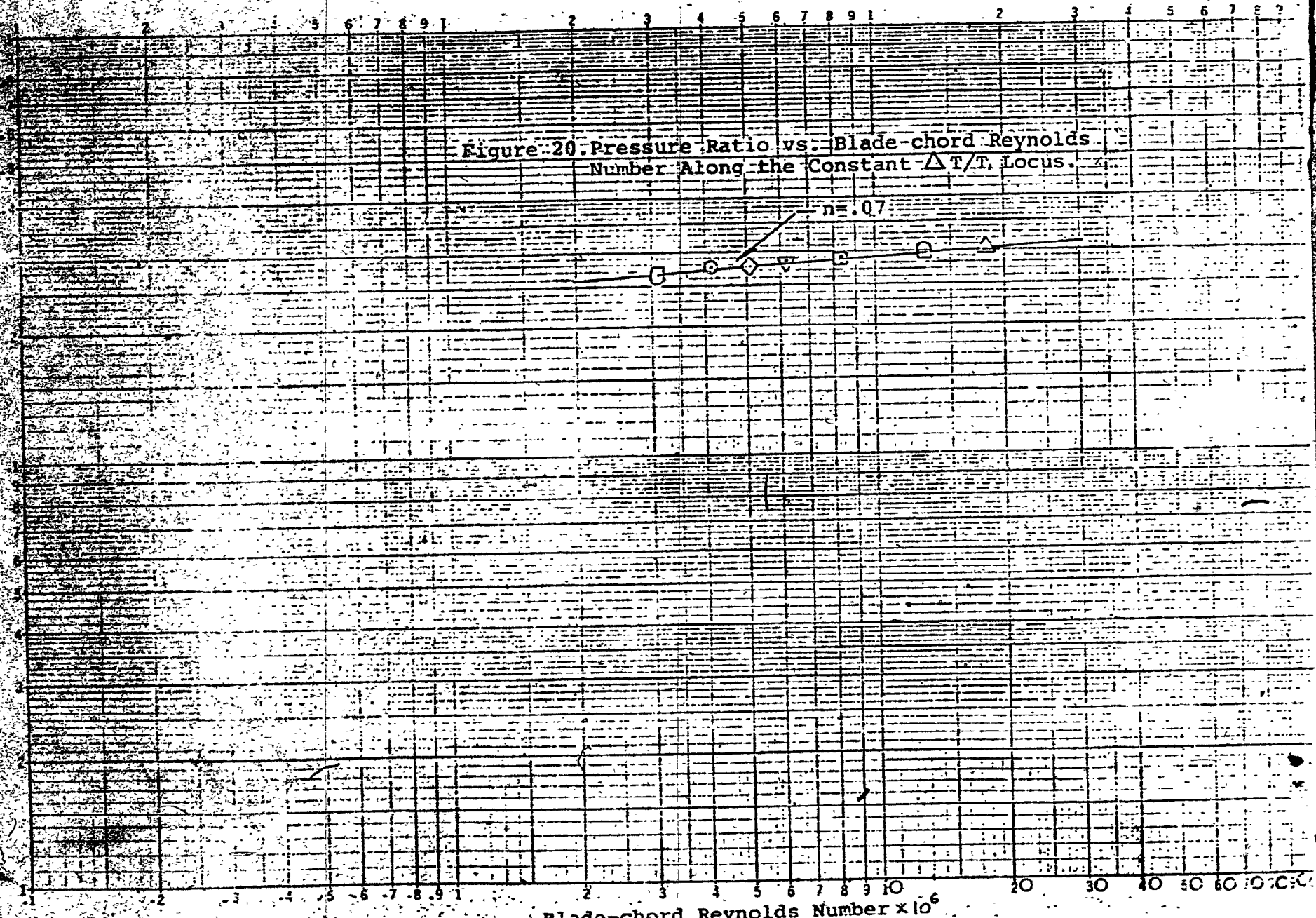

Figure 20. Pressure Ratio vs. Blade-chord Reynolds Number Along the Constant $\Delta T/T_1$ Locus.